ISTANBUL TECHNICAL UNIVERSITY ★ GRADUATE SCHOOL

THE DESIGN OF AN AIRCRAFT ENGINE FAN BLADE BASED ON OPERATIONAL SAFETY REGULATIONS IN CIVIL AVIATION

M.Sc. THESIS

Mert YAĞIZ

Department of Mechanical Engineering

Mechanical Design Programme

SEPTEMBER 2022

ISTANBUL TECHNICAL UNIVERSITY ★ GRADUATE SCHOOL

THE DESIGN OF AN AIRCRAFT ENGINE FAN BLADE BASED ON OPERATIONAL SAFETY REGULATIONS IN CIVIL AVIATION

M.Sc. THESIS

Mert YAĞIZ
503181211

Department of Mechanical Engineering

Mechanical Design Programme

Thesis Advisor: Asst. Dr. Zeynep Parlar

SEPTEMBER 2022

ISTANBUL TEKNİK ÜNİVERSİTESİ ★ LİSANSÜSTÜ EĞİTİM ENSTİTÜSÜ

UÇAK MOTORUNA KUŞ ÇARPMASI DURUMU İÇİN MOTOR PERVANESİ KANATLARININ SİVİL HAVACILIK GÜVENLİK YÖNERGELERİNE UYGUN TASARIMI

YÜKSEK LİSANS TEZİ

Mert YAĞIZ
503181211

Makine Mühendisliği Anabilim Dalı

Konstrüksiyon Programı

Tez Danışmanı: Dr.Öğr.Üyesi Zeynep Parlar

EYLÜL 2022

Mert YAĞIZ, a M.Sc. student of İTU Graduate School student ID 503181211 successfully defended the thesis/dissertation entitled "THE DESIGN OF AN AIRCRAFT ENGINE FAN BLADE BASED ON OPERATIONAL SAFETY REGULATIONS IN CIVIL AVIATION", which he prepared after fulfilling the requirements specified in the associated legislations, before the jury whose signatures are below.

Thesis Advisor :	**Asst. Dr. Zeynep Parlar** İstanbul Technical University	.....
Jury Members :	**Assoc. Dr. Atakan Altınkaynak** Istanbul Technical University	.....
	Prof. Dr. Cüneyt Fetvacı Istanbul University	.....

Date of Submission : 07 September 2022
Date of Defense : 13 September 2022

To a better future,

FOREWORD

I would like to express my gratitude to my esteemed teacher, Prof. Zeynep Parlar, Res. Asst. İsmail Kaya, my dear family, and friends who guided and supported me throughout the thesis process.

September 2022

Mert YAĞIZ
Manufacturing Engineer

TABLE OF CONTENTS

Page

SYMBOLS

ω_d	: Ductile criterion
ω_s	: Shear criterion
ε	: Plastic strain
η	: Stress triaxiality
d_x	: Failure parameters
θ	: Current temperature
$\hat{\theta}$	: Nondimensional temperature
θ_{melt}	: Melting temperature
$\theta_{transition}$	: Transition temperature
θ_S	: Shear stress ratio
p	: Pressure stress
q	: Equivalent stress
τ_{max}	: Maximum shear stress
k_s	: Material parameter

LIST OF TABLES

Page

LIST OF FIGURES

Page

THE DESIGN OF AN AIRCRAFT ENGINE FAN BLADE BASED ON OPERATIONAL SAFETY REGULATIONS IN CIVIL AVIATION

SUMMARY

Since the invention of airplanes, maintaining safe and reliable flights have been one of the prioritized factors to be ensured. The requirement of an aircraft being relatively lightweight to minimize fuel consumption and take advantage of the lift forces brought a series of challenges during both the design and manufacturing stages. Considering the fact that the civil aviation industry has a general purpose of having a profitable business plan, economic criteria such as initial investment of purchasing an aircraft, fuel consumption, cost of regular and unexpected maintenance periods, and employing and training qualified staff to carry out the maintenance actions are important factors hence research and development efforts in this area are mainly geared towards finding a sustainable, safe and affordable middle ground.

As civil aviation as an industry is relatively a new and unfounded concept compared to land route and naval transportation, the majority of the shortcomings of the methods used became known during the trial-and-error approach. Early implementations of both the design and operation methods showed that maintaining the integrity of the aircraft is a challenging task. Apart from engineering an efficient and performant aircraft, ensuring that the harsh operation conditions do not compromise the safety and reliability targets initially set. One of the most important aspects of maintaining the aircraft's safety and structural integrity is preventing external objects from contact in contact with the airplane's exterior. While the types of potentially harmful foreign objects may differ with operational conditions and location, the majority of the objects are globally problematic such as debris, dust, and most importantly birds.

In order to have a better understanding of the nature of bird strike events, bird strike statistics from the previous years are examined and the most likely scenarios that may cover the widest scope are determined. Considering the fact that the probability of a bird strike event happening at cruise altitude where the relative velocity of the bird and the airplane is at maximum, is very low even though it is the most harmful scenario; data from the take-off and climb stages of the flight are examined more closely.

The computer-aided engineering software ABAQUS is used to perform the simulations. The reference bird model is designed based on the previous bird strike event history and literature review on the subject. To validate that the impact model is set up correctly and the impact damage is accurate, a reference aluminum plate with 4 different thickness values was struck with the reference bird model. The primary focus of this study, which is optimizing the design of the fan blades based on how much impact damage a blade can withhold without being rendered inoperative, was targeted toward optimizing the leading-edge design of the blade at the %80 of height from the fan hub which is where most of the bird strike impacts affect.

Within the scope of this study, in which the methods of reducing damage to the fan blades are investigated, 2 different bird models were designed and collided with 7

different fan blade models at 2 different sections. Although the wing models have similar design philosophies in general, the angles of the profiles in the region where the height measured from the wing base are 80% have been changed so that they have different angles of attack during the collision. In this way, although a design similar to the engine blades of turbofan engines currently used in civil aviation is preserved, it is aimed to examine the general damages that occur on the fan blade surface when the profile angle increases or decreases.

UÇAK MOTORUNA KUŞ ÇARPMASI DURUMU İÇİN MOTOR PERVANESİ KANATLARININ SİVİL HAVACILIK GÜVENLİK YÖNERGELERİNE UYGUN TASARIMI

ÖZET

Uçakların icadından bu yana, uçuşların emniyetli ve güvenilir bir şekilde gerçekleşmesi, yerine getirilmesi gereken en önemli ve öncelikli unsurlardan biri olmuştur. Yakıt tüketimini en aza indirmek ve kaldırma kuvvetlerinden en efektif biçimde yararlanabilmek için bir uçağın mümkün olduğu kadar hafif olması gereksinimi hem tasarım hem de üretim aşamalarında bir dizi zorluğu beraberinde getirmiştir. Sivil havacılık sektörünün ve havayolu şirketlerinin öncelikli amaçlarından birinin kârlı bir iş planına sahip olmak olduğu gerçeğinden hareketle, uçakların satın alım veya kiralanması için gerekli ilk yatırım, yakıt tüketimi, düzenli ve beklenmedik bakım süreçlerinin maliyeti, gerçekleştirecek nitelikli personel istihdamı ve yetiştirilmesi gibi ekonomik kriterler, karlılık ve sürdürülebilirlik açısından önemli faktörlerdir. Dolayısıyla bu alandaki araştırma ve geliştirme çabaları esas olarak sürdürülebilir, güvenli ve düşük maliyetli bir orta yol bulmaya yöneliktir.

Sivil havacılığın bir taşımacılık endüstri olarak kara yolu ve deniz taşımacılığına göre nispeten yeni ve daha temelsiz bir kavram olması nedeniyle, kullanılan yöntemlerin eksiklikleri deneme yanılma yaklaşımıyla ortaya çıkmıştır. Hem tasarım hem de işletim yöntemlerinin ilk uygulamaları, uçakların kullanım operasyon ömürleri boyunca güvenli ve düşük maliyetli bir operasyon sunabilmesinin korumasının zorlu bir görev olduğunu göstermiştir. Verimli ve performanslı bir hava aracı tasarlamanın yanı sıra, zorlu çalışma koşullarının başlangıçta belirlenen güvenlik ve güvenilirlik hedeflerinden ödün vermemesini sağlamak yerine getirilmesi gereken en önemli ve en zorlu gereksinimlerden biri olmuştur. Uçakların güvenliğini ve yapısal bütünlüğünü korumanın en önemli yönlerinden biri, hava operasyonları süresince harici nesnelerin uçak ile temas etmesi nedeniyle meydana gelebilecek hasarları engellemek olmuştur. Potansiyel zararlı yabancı unsurların türleri, uçakların operasyon şartlarına ve konumlarına göre farklılıklar gösterebilse de bu tür yabancı unsurların büyük bir bölümünü kuşlar oluşturmaktadır.

Uçaklara operasyon sırasında kuş çarpması durumunda uçağın tüm dış yapısı zarar görebilecek olsa da bu çalışma kapsamında motor pervanelerindeki tekil fan kanatlarının durumları incelenmiştir. Kuş çarpması sürecini ve sonrasında uçaklarda gerçekleşebilecek potansiyel hasarları daha iyi anlayabilmek için önceki yıllara ait kuş çarpması istatistikleri incelenmenmiş ve geniş kapsamda analiz yapılabilmesine olanak sunacak en olası senaryolar belirlenmiştir. Kuş ve uçağın göreli hızının maksimum olduğu seyir irtifasında kuş çarpması olaylarının meydana gelme olasılığının, kuşların uçuş irtifasında barınabilme ihtimalinin düşük olması nedeniyle inceleme altına alınmamıştır. Uçuşun kalkış ve tırmanış aşamalarından elde edilen veriler bu sebep nedeniyle daha yakından incelenmiştir.

Simülasyonları gerçekleştirmek için bilgisayar destekli mühendislik yazılımı ABAQUS kullanılmıştır. Referans kuş modeli, önceki kuş çarpması olaylarının geçmişine ve konuyla ilgili literatür taramasına dayalı olarak tasarlanmıştır. Çarpışma modelinin doğru kurulduğunu ve darbe hasarının tutarlı olduğunu doğrulamak amacıyla, yaplın literatür araştırmaları kapsamında tespit edilen hem analitik hem pratik çarpışma analizi sonuçları içeren referans bir çalışma tespit edilerek analitik edilerek analik sonuçlar üzerinden karşılaştırma yapılmıştır. Referans çalışmada hazırlanan deney düzeneği; kullanılan mesh boyutu ve sayısı, atılan cismin boyutları, malzemesi ve hızı, hedef olarak kullanılan rijit bloğun boyutları ve malzemesi özellikleri gibi parametreler referans çalışmadaki değerler ile aynı olacak şekilde ABAQUS ortamında yeniden oluşturulmuş ve aynı simülasyon koşullarında yapılan analizler sonucunda %5'ten daha düşük bir hata payı elde edilerek hazırlanan ve hazırlanacak olan deney düzeneklerinin isabetliliği ve hassasiyeti doğrulanmıştır. Yapılan analizin doğruluğunun kullanılan mesh boyutundan bağımsızlığını doğrulamak amacıyla mesh sayılarını arttırarak ve azaltarak 2 ek analiz daha yapılmış ve orijinal mesh boyutlarının kullanıldığı çalışma ile karşılaştırılmıştır. Mesh sayısının arttırılmasıyla, deneysel çalışma sonucunda elde edilen değerlere daha da yaklaşılarak hata payı azaltılsa da analizlerin tamamlanması için gerekli sürenin büyük ölçüde artması sebebiyle gelecek analizlerde orijinal mesh boyutlarına sadık kalınmasına karar verilmiştir.

Pervane kanatlarının tasarımını, bir kanadın operasyona devam edemez duruma gelmeden ne kadar darbe hasarına karşı koyabileceğine göre optimize etmek olan bu çalışmanın ana odak noktası olmuştur. Kuş çarpması olayının kanatlara olan etkisinin kanatların pervane göbeğinden uzak bölgelerinde maksimum olması nedeniyle çarpışma bölgesi bu durum göz önüne alınarak belirlenmiştir. Pervane kanatlarındaki hasarı azaltma metotlarının araştırıldığı bu çalışma kapsamında 1.8 kg ve 3.6 kg ağırlıklarına sahip 2 farklı kuş modeli tasarlanarak 7 farklı kanat modeli ile çarpıştırılmıştır. Kanat modelleri genel anlamda benzer tasarım felsefelerine sahip olsa da kanat dibinden ölçülen yüksekliğinin %80 olduğu bölgedeki profillerin açıları değiştirilerek çarpışma sırasında farklı hücum açılarına sahip olmaları sağlanmıştır. Bu sayede, an itibariyle sivil havacılıkta kullanılmakta olan turbofan motorların motor kanatlarına benzer bir tasarım korunmakla birlikte, hücum açısının arttığı ve azaldığı durumlarda kanatlarda meydana genel hasarların incelenmesi hedeflenmiştir.

Yapılan analizlerde malzemelerin hasar dinamikleri simülasyona aktarabilmek amacıyla Johnson-Cook hasarı parametreleri kullanılmıştır. İncelenecek olan çarpışmaların yüksek hızda gerçekleşmesi sonucunda ortaya çıkan yüksek gerilme değerleri, kuş modellerinde kullanılacak malzemenin çarpışma sırasında sıvı karakteristiğine bürünmesini sağlayacağından, kuş modelleri düzleştirilmiş tanecik hidrodinamiği (SPH) metotları kullanılarak oluşturulmuştur.

Motor kanatlarında meydana gelen ön kenar ve orta bölüm hasarına odaklanan simülasyonlar, kanadın %80 yüksekliğindeki profil açısının arttırılmasının plastik deformasyon dayanıklılığı açısından önemli iyileştirmeler sağladığını göstermiştir. Kanat yüzeylerinde izin verilen toleransların genellikle milimetrenin kesirleri ile tanımlandığı gerçeği göz önüne alındığında, deformasyon dayanıklılığındaki iyileştirmeler hem motor üreticileri hem de havayolu işletmecileri için önemli finansal kazanımlar anlamına gelmektedir.

Mevcut çalışma kapsamında pratik bir test ortamına erişimin olmaması ve numune olarak kullanılacak bir motor kanadı elde etmenin maliyetinin finansal açından erişilebilir olmaması nedeniyle, çarpışma testleri bir simülasyon ortamı ile sınırlandırılmıştır. Kanat geometrisini değiştirmenin olası aerodinamik etkisi bu çalışmanın kapsamının dışında tutulmuştur.

1. INTRODUCTION

Bird strike is one of the most detrimental operational inconveniences which can greatly impact operational safety. While all front-facing components of an aircraft such as radome, cockpit, windshield, wing leading edge, fuselage, and landing gear are susceptible to bird strike damage, as a result of the suction at the inlet of the engine, the most vulnerable part of an aircraft to bird strike damage are inlet fan blades of the engine. Due to operating at extremely high revolutions per minute and directing the air to the inner and latter stages of the engine, minor deficiencies on the fan blades such as cracks, bents at the leading and trailing edges of the blades and dents on the front surface can negatively affect the life span of the blades, the operational safety of the flight and aerodynamic efficiency of the engine [1]. In order to ensure the safety of the airplane during a bird strike event, allowed sustained damage to the fan blades are extremely minimal. A fan blade that sustains a few millimeters of dent or bent damage as a result of a bird strike is generally deemed unserviceable for the airlines and needed to be returned to the blade manufacturer for it to undergo a comprehensive overhaul or permanently labeled as unrepairable.

1.1 Purpose of Thesis

In this study, the main parameter which is going to be investigated is the angle of contact between the bird and the fan blade and how it affects the general structural integrity of the blade. The mentioned angle will be altered by making design changes on a certain part of the blade. Blades that have unique features at the contact area but share considerable similarities in general design principles will be compared under identical conditions to determine whether those changes can impact the structural integrity of the blades and increase their life span while adding no additional material and manufacturing costs.

Due to the nature of the bird strike events, there are some aspects of the impact that are almost random such as the flow path of the air due to the turbulent air in front of the engine, the flight path of the bird, and the exact impact angle between the bird and

the fan blade [2]. The factors such as flight speed of the bird, mass & shape of the bird, cruising speed of the aircraft, RPM value of the engine driveshaft, material of the blades, impact altitude, air & engine temperature are either predictable and can be obtained from observing detailed flight logs of individual operations.

1.2 Motivation

Since the cost of a blade is extremely high and the probability of a bird strike event happening is very high, the annual cost of inspecting, repairing, overhauling or replacing fan blades adds up to enormous costs for both airlines and manufacturers [3]. Any slight improvement to be made for the design of the fan blade that may result in less sustained damage of a fraction of a millimeter bent or dent on the fan blade means millions of dollars of less maintenance or manufacturing costs.

1.3 Literature Review

Even though there are studies in which bird strike event is experimentally observed, there are almost no experiments where crucial aspects and parameters of the striking incident are fully replicated since many of the parameters such as manufacturing dimensions & tolerances of the fan blades and material information of the blades are estimated.

In order to have a better understanding of bird strike events and obtain data for realistic impact parameters such as the most susceptible parts of an aircraft to a bird strike, the most common speed and flight altitude for the impact and weight and size of the projectile, a comprehensive report by European Union Aviation Safety Agency (EASA) was thoroughly examined.

Cwiklak has investigated the maximum strain values of steel and titanium alloy rigid blocks in an event of an artificial bird strike. Maximum stress and strain values are recorded with strain gauges and measurement control computers while being surrounded by high-speed cameras. The gelatin projectile is released from an air pressure gun. The study confirmed that gelatin projectiles showed hydrodynamic behavior during and after the impact and additional porosity in addition to linear EOS of the gelatin projectile contributes to getting more accurate analysis results to the experimental results [4].

In addition to official aviation safety organization reports, the study of Metz et al. shows detailed information regarding the probability of a bird strike event occurring and how initial impact parameters such as bird count and bird size depend on geographical factors [5].

Edge et al. investigated the feasibility of using analytical bird models in bird strike simulations and validated them against experimental data. As a result of the study, predictive techniques in determining the possible aircraft structure damages were deemed feasible [6].

Budgey's study aimed to standardize the geometry of the bird projectiles used in both practical and analytical bird strike studies. Straight-ended cylinder, ellipsoid and hemispherical ended cylinder projectiles were fired by high powered gas cannon at realistic operational velocity towards a reference target and analyzed & compared based and their diameter, length and mass. The motivation of the study was the fact that the cost of using real birds in bird strike studies being expensive, lack of uniformity and the challenge of nullifying the biological factors between individuals of the same species [7].

In Goyal's study, 3 different computational methods (2D & 3D ALE, Lagrangian and SPH) are used in one-dimensional beam-centered bird strike impact scenario. A reference bird model is launched towards a rigid flat plate in an LS-DYNA analysis environment at 30º and 90º degree angles and peak forces are compared with experimental results obtained in the study by Moffat et al (2001). It has been observed that at angled impacts, smooth particles hydrodynamics methods yields %6.96 error while 2D ALE, Lagrangian and 3D ALE results in %11.96, %13.38 and %19.8 errors respectively [8].

Mao et al. studied the effects of the incidence angle between the projectile and the fan blade by altering the direction of the projectile. Within the scope of the study, dynamic responses and deformation damages are observed. It has been concluded that an impact at an incidence angle of 0º yields the maximum plastic deformation. It has also been observed that oscillations of the blade as a result of the impacts contributed to increasing the accumulated plastic strain [9].

Upadhyay et al. mention that increasing the weight of the fan blade assembly lead to an additional 2-2.5 kg increase in aircraft structural weight in the fuselage and the

engine [10]. In addition, Steinegger et al. point out that an additional weight increase for the aircraft results in additional fuel consumption of 0.02 kg fuel per 1000km traveled [11]. Considering both of the studies, it can be concluded at any design alteration results in increasing the weight of the fan blades, therefore the general weight of the aircraft will result in additional material and fuel costs during operation.

It can be concluded from the literature review that very few studies investigated a bird strike situation where multiple individual birds directly hit the fan blade. Similarly, any possible damage to an engine component other than inlet fan blades such as HPT (High-Pressure Turbine), LPT (Low-Pressure Turbine) and combustion chamber was seldomly investigated.

It is observed that excluding the chasing of the engine from the fan blade assembly is a common practice in bird strike simulations. However, Carlsson et al. pointed out that any excessive damage to the fan blade which can tear off material from the fan blade can impact and damage the casing of the engine [12].

2. FAN BLADE DESIGN PARAMETERS

Optimizing the design of an engine fan blade has always been one of the top priorities during the whole engine design process. Because the airplanes used in civil aviation are powered by turbofan engines which take full advantage of the bypass air that is absorbed and directed by the set of fan blades at the front, designing a fan blade set as efficient and optimized as possible is one of the critical steps of the research and development process. Since the civil aviation industry has taken a direction of carrying as many people as possible and cutting operational and maintenance costs ensuring a safe and reliable operation is a top priority, factors such as fuel efficiency, durability, repairability, and initial investments cost are among the most crucial elements of the design process which airlines directly take interest.

2.1 Fuel Efficiency

Minimizing fuel consumption is one of the most critical cost-cutting methods for airlines. This apparent demand from the civil aviation industry has pushed aircraft manufacturers toward designing more fuel-efficient aircraft for their consumers. As observed from new-generation civil transport aircraft, engine manufacturers began to develop engines that can maximize the bypass air by increasing the fan blade diameters of the inlet fans on the engines since the increased amount of intake air results in much fuel-efficient operation [13].

Determining the material of the fan blades is not only crucial for the endurance and longevity of the blades but also plays an important role in the fuel consumption aspect. Aside from the aerodynamic structure of the blade, the choice of material alone can also directly impact the fuel efficiency of the aircraft.

Designing a different fan blade for the aircraft engine also results in substantial changes in the design of the core engine. In order to compensate for a 1 kg increase in the weight of a single fan blade, an additional 2-2.5 kg of weight increase in the aircraft structure, engine structure, containment, and engine rotor have to be added to the aircraft and its engines. These weight increases naturally result in higher fuel consumption as an aircraft needs to be as light as

possible in order to fully upturn its fuel efficiency [14]. Considering the fact that transportation of 1kg additional weight over a distance of 1000 km consumes an additional 0.2kg of fuel, a single new generation double aisle aircraft which are generally used for intercontinental transportation, travels 3.500.000 km on average and consumes more than $100.000 worth of additional fuel.

2.2 Operational Safety

Air transportation is performed in a much more hostile environment compared to other means of transportation. Due to the many external and unique factors that may harm structural integrity, operational safety is the most crucial aspect of designing and developing an airplane component.

In bird strike situations, inlet fan blades are the first key component to be damaged. During a bird strike scenario, the condition of the key components of the core engine heavily depends on the structural integrity of the fan blades. Being the main source of the thrust generation, any substantial damage to the fan blades may result in loss of required thrust, which heavily hinders operational safety.

In order to ensure a standard of safety for fan blade damages during a bird strike scenario, European Aviation Administration requires a general benchmark for airlines to be satisfied. When the aircraft's velocity is equal to V_C at sea level or 0.85 V_C at the altitude of 2438 meters, whichever is more relevant to the situation, the aircraft must be designed to ensure uninterrupted safe flight and landing capabilities after impact with a 4lb bird. Compliance can only be demonstrated by analysis results when tests are performed on sufficiently representative structures of similar design.

2.3 Maintenance and Overhaul Costs

Bird strike is a relatively common occurrence during the operation of an airplane. This frequent event which may critically hinder the structural integrity of the fan blades and the engine in general brings substantial maintenance and overhauls costs. Considering the cost of a single fan blade for a new generation double aisle passenger aircraft can reach up to $100.000, durability and longevity of the fan blades remain as important factors for airlines to consider.

3. IMPACT PARAMETERS

3.1 Fan Blade Damage Types

Fan blade damages that result after the impact of a bird varies based on different parameters. The weight and dimensions of the bird, the relative speed of the impact, and the angle at which the bird hit the blades are some of the main factors that affect how detrimental the damage will occur. Each different damage type has unique impacts on aircraft safety and allowed damages to the different areas of the fan blade to vary based on the regulations aviation safety organizations set [15].

Airplane manufacturers generally divide the front and back faces of the fan blades into different sections in order to precisely set damage allowances and cycle or distance counts for the plane to be able to operate with the damaged fan blade until the damaged section needs repairing or replacing.

3.1.1 Bents and curls

Bends and curls are the types of damage that occur in the fan blade's outer sections called the leading edge and trailing edge. Due to fan blade design, fan blade thickness generally decreases, and any foreign object that may hit the outer section of the blade is more likely to damage the blade [16]. Less than 3mm of tip bents or curls are generally permitted, but fan blades with a leading-edge or trailing-edge bent more than 1.5mm are not serviceable. Due to being frequently observed and sections being capable of bending as a result of bird strikes, bent damages will be investigated within the scope of this study.

3.1.2 Dents and nicks

Inner or middle sections of the fan blade are susceptible to dents and nicks. Increased thickness of the fan blade provides additional strength to the inner sections. Dents with less than 1.5mm of depth are generally accepted except for leading-edge dents making the fan blade unserviceable. Even though dent damages generally have the most

allowed damage tolerance, the highest occurrence frequency among all other fan blade damages will be the reason for its inclusion in this study.

3.1.3 Cracks and tears

Cracks and tears are the most severe damage that can occur due to a bird strike situation. Any crack or tear is not permitted regardless of the width, length, or depth. Compared to other damages, although being the most detrimental, the occurrence frequency of this type of damage is lower, hence this study will not cover any crack or tear damage examination.

3.2 Impact Parameters

Engines are one of the most susceptible parts to bird strike events. Having the utmost critical role in producing the thrust and ensuring the continuity of the flight, optimizing the engine core and fan blades' strength and durability plays a significant role in warranting operational safety. Previously obtained data from the aviation authorities indicate that %25 bird strike events result in significant damage to the aircraft's engine [17]. Although there are previous studies covering the other most bird-strike-damage susceptible sections such as the windshield and fuselage of the plane, damages to the fan blades, or more generally the engine, will be covered within the scope of this study since the functionality of the fan blades play a more important role in preserving the safety of the flight operation [18-19]. Statistical data regarding the occurrence frequency of the bird strike events per aircraft section list is represented in Table 3.1.

Table 3.1 : Percentage of strikes resulting in damage by aircraft section.

Part Struck	Percentage of Strikes	Percentage of Strikes Causing Damage
Nose/Radome/Fuselage	%45,32	%30
Wing/Engine	%21,31	%25
Windshield	%18,05	%9,5
Landing Gear	%11,31	%9,5
Tail	%2,7	%30
Lights	%1,31	%71

3.2.1 Impact model properties

Bird strike occurs at extremely high velocities due to airplanes accelerating at full thrust during the take-off and climb stages of the flight. Due to the high-velocity impact, forces created greatly surpass the tissue strengths of the bird and make the bird act like a non-viscous fluid [20]. During the analysis stage, water is chosen as the primary bird material.

Instances where multiple birds strike the engine simultaneously have a much lesser possibility than a single bird strike. Data and statistics provided by European Aviation Safety Administration show that more than %70 bird strike events are caused by a single bird striking the engine. To cover the most probable event, the analysis result will be based on a single bird striking the fan blades [20]. As shown in Table 3.2, bird strike events involving a single projectile are more common compared to multiple projectile occurrences.

Table 3.2 : The number of birds struck by bird strike event.

Number of Birds	%Strike Probability	%Unserviceable Damage
1	%72	%11.9
2-10	%25	%18.9
>10	%3	%23.8

The mass and diameters of the bird which will be used in the analysis are also chosen for the general purpose of analyzing the most probable scenario [20]. Birds weighted more than 1.8kg covers most of the bird strike occurrences as represented in Table 3.3.

Table 3.3 : Single bird engine strikes causing damage by mass.

Mass Range (kg)	Damage Probability
<0.1	%2.6
0.1-0.45	%4.1
0.45-0.9	%16.3
0.9-1.8	%5
1.8-3.6	%31.6
>3.6	%40.4

3.2.2 Impact velocity

Bird strikes generally take place during the take-off, climb, descent and landing stages of the flights. Due to aircraft flying at almost 8000 ft altitude during the cruise when the aircraft speed is at maximum, impacts at around 900 km/h happen rarely hence 150 m/s (540 km/h) relative impact speed will be chosen for the future simulation in order to imitate the climb stage of the flight. Aircraft speed increases as the aircraft gain altitude hence the force applied onto the blades and the severity of the impact scales up. Table 3.4 provides information regarding the altitude at which an aircraft is more susceptible to damage.

Table 3.4 : Strikes to aircraft by altitude

Altitude (ft.)	Strike Probability	Unserviceable Damage
0	%42.19	%6
0-100	%26.77	%9
100-200	%8.64	%12
200-400	%7.70	%12
400-600	%3.71	%20
600-800	%1,39	%21
800-1000	%1.29	%27
1000-2000	%4,33	%36
2000-8000	%3,98	%52
>8000	%0.32	%67

3.3 Dynamic Analysis Parameters

3.3.1 CAE tools

The CAE tool chosen ABAQUS is an industry-specific, integrated finite element software. In addition to being used in a wide variety of industries such as aviation, automotive, construction, and the medical sector, it also meets the analysis needs of scientific research. With ABAQUS, events covering many different fields, from very simple linear problems to the most difficult complex problems, can be simulated. As a result of covering a wide variety of material models and finite element types it offers, it provides the users with the opportunity to effectively analyze linear and non-linear

large-scale projects, which are difficult to solve with classical methods, using the finite element method.

3.3.2 Analysis formulations

The information previously mentioned regarding the parameters of the bird and the fan blade will be used for the complex dynamic analysis by the CAE software ABAQUS. Bird properties such as density, equation of state (EOS), dynamic viscosity, and blade properties such as young modulus, stress-strain rate information, stress triaxiality, fracture strain, and stress rate are needed to be provided to the CAE software in order to accurately replicate a real-world bird strike event.

3.3.2.1 Material information

In order to simulate a low-viscosity characteristic as a result of a high velocity impact of the bird to a fan blade, the material properties of the fan blade will be chosen as titanium alloy Ti6Al4V which is closer and more accurate to the real-world applications. General material properties and Johnson-Cook parameters of the chosen material are presented at Table 3.5 & Table 3.6 [21].

Table 3.5 : General material parameters of the fan blade material

Density (kg/m^3)	*Young's Modulus [MPa]*	*Poisson's Ratio [-]*
7.850×10^3	2.1×10^8	0.3

Table 3.6 : Johnson-Cook parameters of the fan blade material

A (MPa)	*B (MPa)*	*n*	*c*	*m*
782.7	498.4	0.28	0.028	1

3.3.2.2 Ductile damage information

Predictions regarding the possible damages due to projectile strikes use information such as the unification of voids, nucleation, and growth [22-23]. The algorithm calculates the plastic strain at the starting point using parameters such as strain rate and stress triaxiality. The equation can be written as follows;

$$\bar{\varepsilon}_{\mathrm{D}}^{pl}(\eta, \dot{\bar{\varepsilon}}^{pl}) \tag{3.1}$$

Where p represents the pressure stress, q is the Mises equivalent, the equation '$\eta = -\mathrm{p}/\mathrm{q}$' expresses the stress triaxiality while $\dot{\bar{\varepsilon}}^{\mathrm{pl}}$ is the equivalent plastic strain rate. If the following condition is satisfied, the damage initiation process begins.

$$\omega_{\mathrm{d}} = \int \frac{\bar{\varepsilon}^{\mathrm{pl}}}{\bar{\varepsilon}_{\mathrm{D}}^{\mathrm{pl}}(\eta, \dot{\bar{\varepsilon}}^{\mathrm{pl}})} = 1 \tag{3.2}$$

Plastic deformation increases in parallel with ω_{d}, the state variable. Each incremental increase in ω_{d} is calculated as,

$$\Delta\omega_{\mathrm{d}} = \frac{\Delta\bar{\varepsilon}^{\mathrm{pl}}}{\bar{\varepsilon}_{\mathrm{D}}^{\mathrm{pl}}(\eta, \dot{\bar{\varepsilon}}^{\mathrm{pl}})} \geq 0 \tag{3.3}$$

3.3.2.3 Johnson-Cook equation

The Johnson-Cook equation different method for the calculation of ductile criterion where the applied stress and the damage initiation grows at the same time.

$$\bar{\varepsilon}_{\mathrm{D}}^{pl} = [d_1 + d_2 \exp(-d_3\eta)]\left[1 + d_4 \ln\left(\frac{\dot{\bar{\varepsilon}}^{pl}}{\dot{\varepsilon}_0}\right)\right](1 + d_5\hat{\theta}) \tag{3.4}$$

d_1 to d_5 represents the failure parameters and $\dot{\varepsilon}_0$ is the reference strain rate.

$$\hat{\theta} \equiv \begin{cases} 0 & \text{for } \theta < \theta_{transition} \\ (\theta - \theta_{transition})/(\theta_{melt} - \theta_{transition}) & \text{for } \theta_{transition} \leq \theta \leq \theta_{melt} \\ 1 & \text{for } \theta > \theta_{melt} \end{cases} \tag{3.5}$$

θ symbolizes the current temperature while θ_{melt} is the melting temperature and $\theta_{transition}$ is the transition temperature. Since the temperatures at the low-pressure combustor exit stage are generally measured at around 200 ºC which is much cooler compared to the transition temperature of the fan blade material (~970 ºC), inlet fan assembly engine which is closer to the ambient inlet air and farther from the combustion chamber is not affected from the temperature [24-25].

3.3.2.4 Shear damage

The shear criterion is a phenomenological model for predicting the onset of damage due to shear band localization. The model assumes that the equivalent plastic strain at the onset of damage, $\bar{\varepsilon}_S^{pl}$, is a function of the shear stress ratio and strain rate.

$$\bar{\varepsilon}_S^{pl} = (\theta_S, \dot{\bar{\varepsilon}}^{pl}) \tag{3.6}$$

$$\theta_S = (q + k_s p)/\,\tau_{max} \tag{3.7}$$

θ_S symbolizes the stress ratio, τ_{max} is the maximum shear stress and k_s is the material constant. Shear damage can be observed if the following equation's condition is met.

$$\omega_s = \int \frac{d\bar{\varepsilon}^{pl}}{\bar{\varepsilon}_S^{pl}(\theta_S, \dot{\bar{\varepsilon}}^{pl})} = 1 \tag{3.8}$$

where ω_s is a state variable that increases with plastic deformation relational to the cumulative change in equivalent plastic strain. The continuing increase in ω_s is computed as

$$\Delta\omega_S = \frac{\Delta\bar{\varepsilon}^{pl}}{\bar{\varepsilon}_S^{pl}(\theta_S, \dot{\bar{\varepsilon}}^{pl})} \geq 0 \tag{3.9}$$

In an explicit dynamic analysis with the ABAQUS software, the shear criterion can be used with the Johnson-Cook damage equation.

3.3.2.5 Impact model

As a result of the nature of an organic projectile hitting a solid body at extreme velocity, stress generated by the impact exceeds the material strength and projectile acts like a fluid [26]. In order to simulate this phenomenon during the analysis, smooth particles hydrodynamics method is used.

Due to the occurrence of significantly large deformations on the bird body, usage of the smooth particle hydrodynamics suits a bird strike situation yields more accurate results compared to the mesh smoothing technique. Large distortions of the finite element mesh make the mesh smoothing technique in a bird strike scenario less preferable [27]. Solid finite element meshes are replaced with a set of discrete interacting particles in meshless Lagrangian SPH technique.

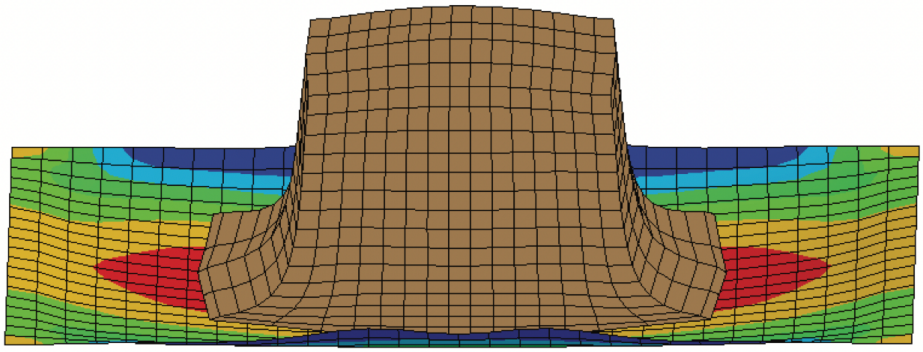

Figure 3.1 : Fluid mesh smoothing method during impact.

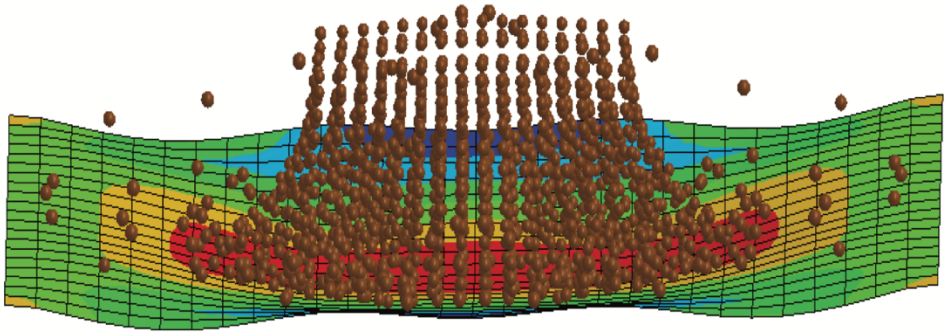

Figure 3.2 : Smooth particle hydrodynamics method during impact.

4. BIRD STRIKE SIMULATION

4.1 Analysis Verification

In order to validate the accuracy and the preciseness of the future work performed on the different sets of fan blades, experimental results obtained from the experimental work of Cwiklak et al. will be compared with the ABAQUS analysis results by designing the exact experiment environment and finite elements analysis input from the mentioned work. Similar to the mentioned work, a reference steel plate with dimensions 0.5 × 0.5 × 0.1 m was positioned as a rigid target and a projectile which is 212 mm in length & 106 mm in diameter weighed at 1.81 kg was shot at the rigid target at 116 m/s velocities [4]. The designed reference bird & plate model is represented in Figure 4.1 & Figure 4.2.

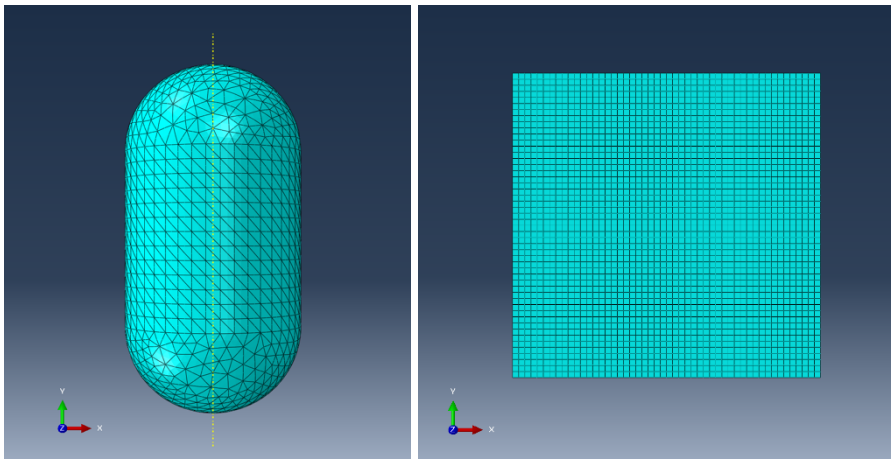

Figure 4.1 : Designed reference bird & plate model.

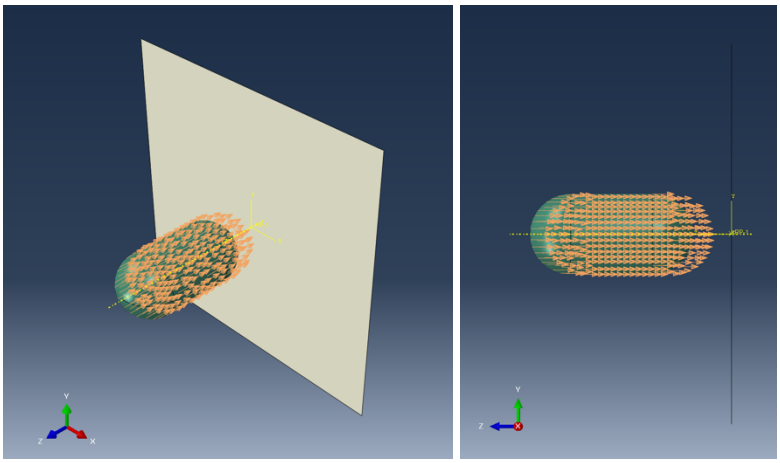

Figure 4.2 : Isometric & front view of the reference plate design model

Similar to the finite element analysis section of the related work, the reference rigid steel plate consists of exactly 2500 elements as its reference while the bird projectile consists of 15252 elements compared to 15216 used in the original work. Material properties of the steel blade and the bird model are presented in Table 4.1, Table 4.2 & Table 4.3 [28].

Table 4.1 : EOS parameters of the bird model.

Bulk Speed of Sound (m/s)	*Linear Coefficient (-)*	*Quadratic Coefficient (-)*	*Cubic Coefficient (-)*	*Gamma (-)*
1.438	1.92	0	0	0.1

Table 4.2 : Material parameters of the bird model.

Density (kg/m^3)	*Cut-Off Pressure [Pa]*	*Viscosity Coefficient [Pa.s]*
950	-10^6	0.001

Table 4.3 : Material properties of the steel plate.

Density (kg/m^3)	*Young's Modulus [MPa]*	*Poisson's Ratio [-]*
7.850×10^3	2.1×10^8	0.3

Since the main objective of this study is to research the plastic deformations and the strains that occurred on the fan blades, the experimental strain value obtained is

compared with the analytical results of the study. According to the experimental results, the reference rigid body yielded a maximum strain value of 7.95 × 10−4 mm while the analysis results outputted the maximum strain value as 7.63 × 10−4 mm which yields an error percentage of less than 5%.

Node: PLATE-1.1302

	1	2	3	Magnitude
Base coordinates:	-1.00000e+01,	0.00000e+00,	0.00000e+00,	-
Scale:	1.00000e+00,	1.00000e+00,	1.00000e+00,	-
Deformed coordinates (unscaled):	-9.99999e+00,	-2.80142e-06,	7.62939e-04,	-
Deformed coordinates (scaled):	-9.99999e+00,	-2.80142e-06,	7.62939e-04,	-
Displacement (unscaled):	9.53674e-06,	-2.80142e-06,	7.62939e-04,	7.63004e-04

Figure 4.3 : ABAQUS output of maximum deformation on the reference plate (10mm x 10mm mesh size)

ABAQUS output presented in Figure 4.3 provides information regarding the base coordinates of the impact point of the plate before and after sustaining plastic deformation. The displacement value represents the magnitude of dent or bent appearing on the blade.

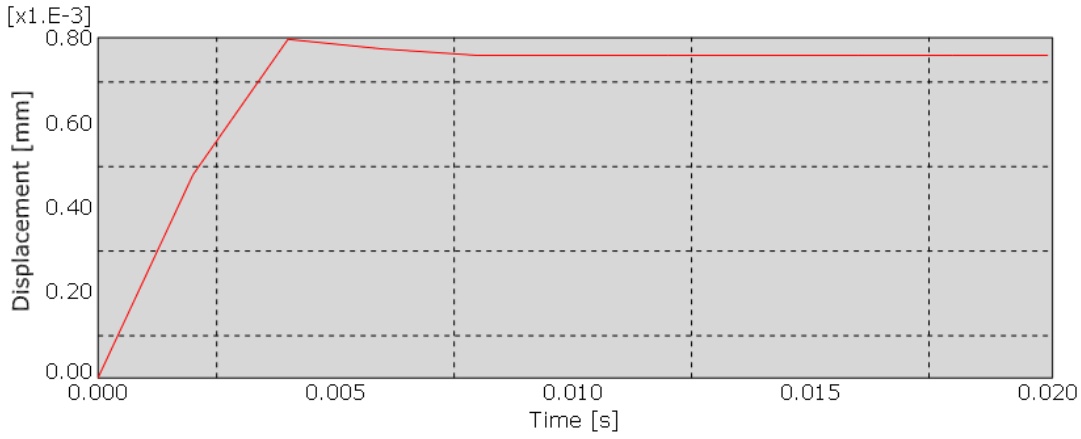

Figure 4.4 : Nodal displacement graph of the impact point

Nodal displacement data presented in Figure 4.4 indicates the amount of elastic deformation occurring in the impact zone. Quick and total dissipation of the elastic deformation on the rigid plate is a result of its high thickness.

4.2 Mesh Independence

In order to isolate the mesh size and amount from the analysis results, the same analysis setup was reused with 5 mm x 5 mm & 20 mm x 20 mm sized meshes. The initial mesh size of 10 mm x 10 mm was multiplied and divided by the least common denominator ‘x2’ in order to precisely preserve the initial impact point.

Node: PLATE-1.5103

	1	2	3	Magnitude
Base coordinates:	-1.00000e+01,	0.00000e+00,	0.00000e+00,	-
Scale:	1.00000e+00,	1.00000e+00,	1.00000e+00,	-
Deformed coordinates (unscaled):	-9.99999e+00,	-7.74860e-07,	-7.78198e-04,	-
Deformed coordinates (scaled):	-9.99999e+00,	-7.74860e-07,	-7.78198e-04,	-
Displacement (unscaled):	6.19888e-06,	-7.74860e-07,	-7.78198e-04,	7.78223e-04

Figure 4.5 : ABAQUS output of maximum deformation on the reference plate (5 mm x 5 mm mesh size)

Node: PLATE-1.351

	1	2	3	Magnitude
Base coordinates:	1.00000e+01,	-1.00000e+01,	0.00000e+00,	-
Scale:	1.00000e+00,	1.00000e+00,	1.00000e+00,	-
Deformed coordinates (unscaled):	9.99999e+00,	-1.00000e+01,	-3.66211e-04,	-
Deformed coordinates (scaled):	9.99999e+00,	-1.00000e+01,	-3.66211e-04,	-
Displacement (unscaled):	-6.67572e-06,	-1.54972e-06,	-3.66211e-04,	3.66275e-04

Figure 4.6 : ABAQUS output of maximum deformation on the reference plate (20 mm x 20 mm mesh size)

According to the analysis results as presented in Figure 4.5 & Figure 4.6, despite using a finer mesh structure increased the precision of the results by yielding displacement values closer to the experimental results, an almost 250% increase in the time required to conclude the analysis was observed. An increase in the analysis run times was too big for the negligible increase in precision, hence all future analyses in this study will be performed with 10 mm x 10 mm sized meshes.

4.3 Fan Blade and Bird Model Design

Inlet fans consisting of 22 individual blades with dimensions of 121.9 mm x 58.4 mm x 43.2 mm are designed for the primary analysis. In order to reduce the computational power needed for the analysis, fan blades that are not in direct contact with the projectile were left unmeshed. 2 different hemispherical bird models with similar dimensions compared to the study mentioned during analysis verification, weighted at 1.8 kg & 3.6 kg were used.

Due to the angle of attack and increased stiffness, impact forces are expected to be lesser near the blade hub, while the areas near the tip of the blade are more susceptible to damage. As a result of the curvature of the edges and the area differences between the tip and the hub, the tips of the blades are stressed more than the areas nearing the hub, which means damages due to impact and overall strain are greater on the tip areas. Considering this criterion, the area of impact is chosen at %80 blade height.

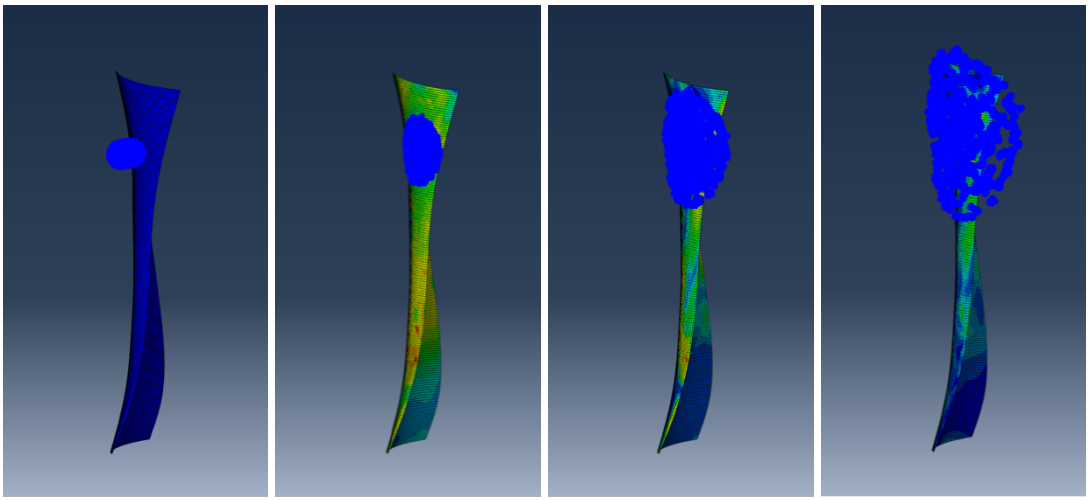

Figure 4.7 : Isometric view of the projectile hitting the fan blade.

Directions of the projectiles were always chosen in a parallel direction with the center of the inlet cone. The angle at which the projectile will hit against the plate is going to differ with the facial curvature of each individual set of blades. Initial simulations also confirm the hydrodynamic behaviors of the SPH method as visualized at Figure 4.7. Material properties of the titanium alloy will remain constant throughout all analyses and are presented in Table 3.5 & Table 3.6.

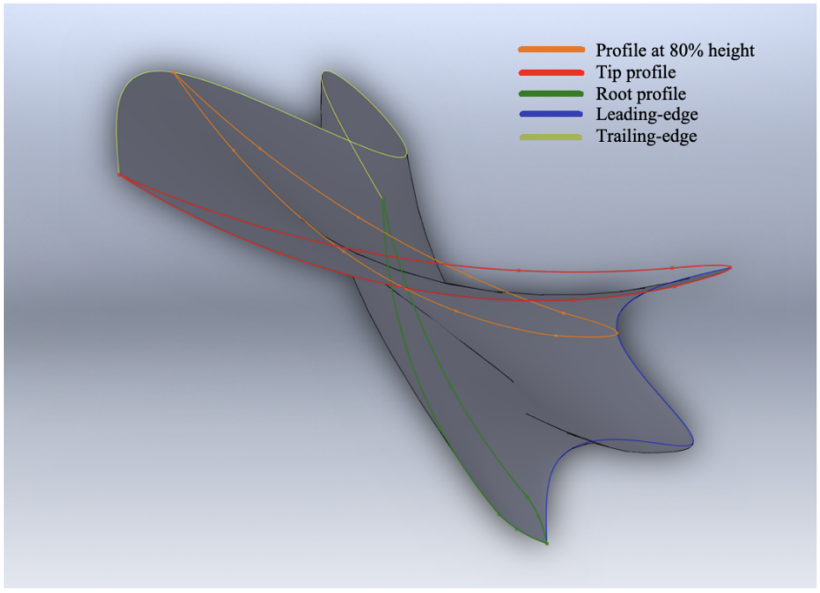

Figure 4.8 : Top view of the reference fan blade profile at 80% height.

Trailing-edge, leading edge, root and tip sections of the fan blade are presented at Figure 4.8. The design of the other 6 fan blade designs which will be analyzed within the scope of this study, will be based on the design of the reference blade. Compared

to the reference blade, 2 of the 6 iterations are generated by rotating the blade profile at 80% height counter-clockwise by 10º in total with 2 equal 5º increments (Figure 4.9 – Subfigure a: -10º & b: -5º) and the other 4 of the 6 iterations are created by rotating the same blade profile clockwise by 20º in total with 4 equal 5º increments (Figure 4.10 – Subfigure c: 5º, d: 10º, e: 15º & f: 20º).

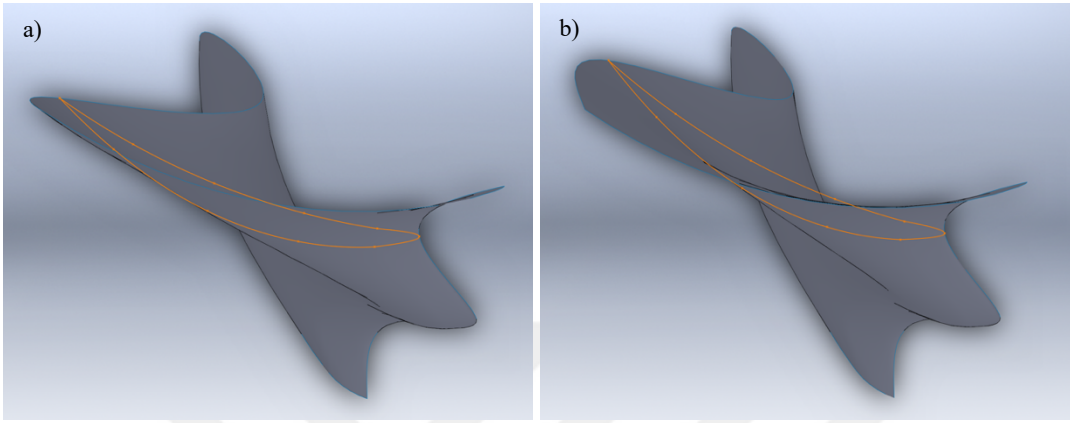

Figure 4.9 : Top views of the fan blade profiles rotated counter-clockwise by 5º respectively

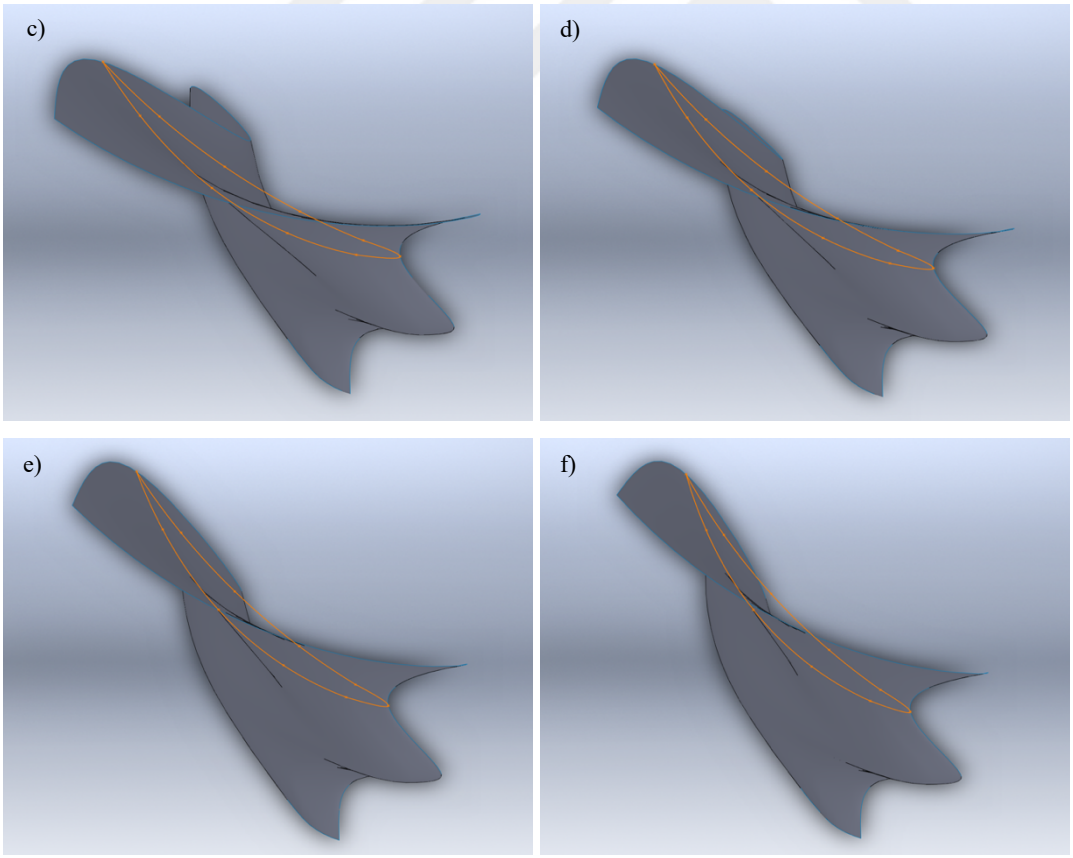

Figure 4.10 : Top views of the fan blade profiles rotated clockwise by 5º respectively

As it can be observed from the top view of fan blade designs, the only difference between each fan blade is the angle between the blade profile at 80% height and the incoming projectile. This results in changing the incidence angle without changing the direction of the profile. In ABAQUS analyses, instead of deformable solid parts, a shell-based feature is used in order to reduce the time required to conclude the analysis results faster.

5. RESULTS

7 fan blade designs with different contact angles at 80% height were submitted for analysis. Profile angle difference between each fan blade design was at most 30º with an increase 5º between most similar designs. In order to obtain the most two common types of deformation after a bird strike event, which are bending at the leading edge and denting on the middle sections, 2 different impact locations were chosen.

In order to study the bending and denting behavior after a bird strike, the impact location is chosen closer to the leading edge of the fan blade for the bending and near the center of the fan blade for the denting observations. For each study, 7 different impact scenarios with 7 different fan blades have been simulated and plastic deformations at the edge of the leading edge of the fan blade have been compared. In comparison, the unique nodal spatial displacement values in millimeters between the original location of the most deformed node and the final location of the node are used after elastic deformations, oscillations and vibrations are dissipated.

The thickness of the shell model is set at 15mm. Projectiles which are 200 mm in length & 100 mm in diameter and 200 mm in length & 15 mm in diameter weighted at 1.8 kg & 3.6 kg were shot at the rigid target at 150 m/s velocity. Single mesh elements size of each fan blade is set at 10mm x 10mm while the bird model is prepared with 1245 nodes meshlessly using SPH method. Mesh structures of the fan blades are chosen as structured. Root profiles of the fan blades are fixed at the ends as encastre. Material properties of the titanium alloy are presented in Table 3.5 & Table 3.6.

In modern turbofan engine fan blades, a blade design philosophy with 10º-15º of profile angle at 80% height is generally observed. By analyzing multiple angle variations between 0º-30º, any improvements or diminishments in terms of maximum plastic deformations will be studied.

5.1 Bending at the Leading Edge of the Fan Blade with a 1.8 kg projectile

Analyses were conducted in order to simulate a 1.8 kg projectile hitting a fan blade at the leading-edge section. Figures from 5.1 to 5.7 represent the visuals of the blade before and after each impact simulation as well as the ABAQUS outputs regarding the displacement of the node which sustained the most plastic deformation in relation to its original position. Profile angle to nodal displacement graph is shown at Figure 5.8.

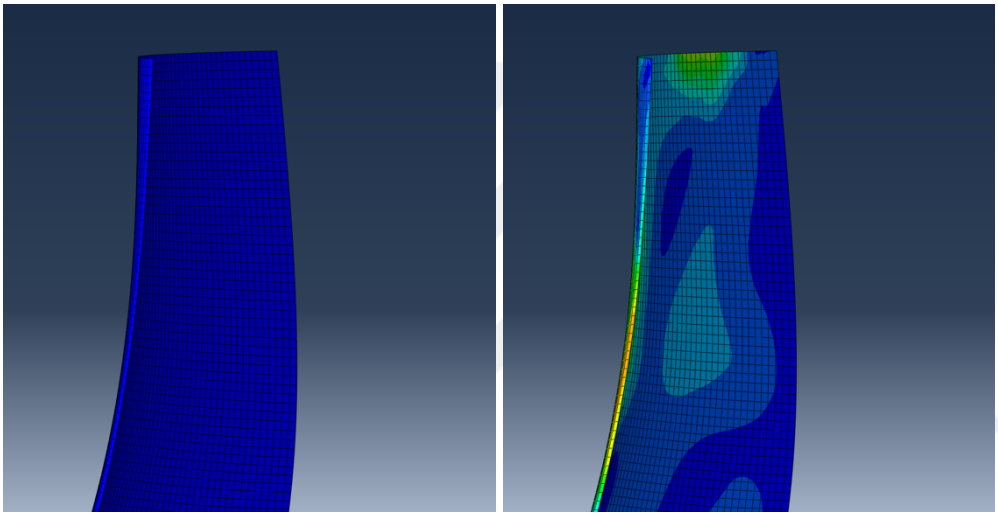

Node: P10-1.7554

	1	2	3	Magnitude
Base coordinates:	1.14269e+02,	7.42490e+02,	1.14213e+02,	-
Scale:	1.00000e+00,	1.00000e+00,	1.00000e+00,	-
Deformed coordinates (unscaled):	1.15810e+02,	7.42490e+02,	1.14213e+02,	-
Deformed coordinates (scaled):	1.15810e+02,	7.42490e+02,	1.14213e+02,	-
Displacement (unscaled):	1.54102e+00,	0.00000e+00,	0.00000e+00,	1.54102e+00

Figure 5.1 : ABAQUS output of maximum deformation at the impact at -10º

Base coordinates represent the location of the impact before any deformation occurring while deformed coordinates indicates the updated coordinates of the chosen fan blade node where the projectile makes its initial contact during impact. Displacement value shows the coordinal location difference between the undeformed and deformed node in millimeters. As presented at Figure 5.1, at an angle of -10º to the reference design, the displacement of the chosen node is 1.54 mm.

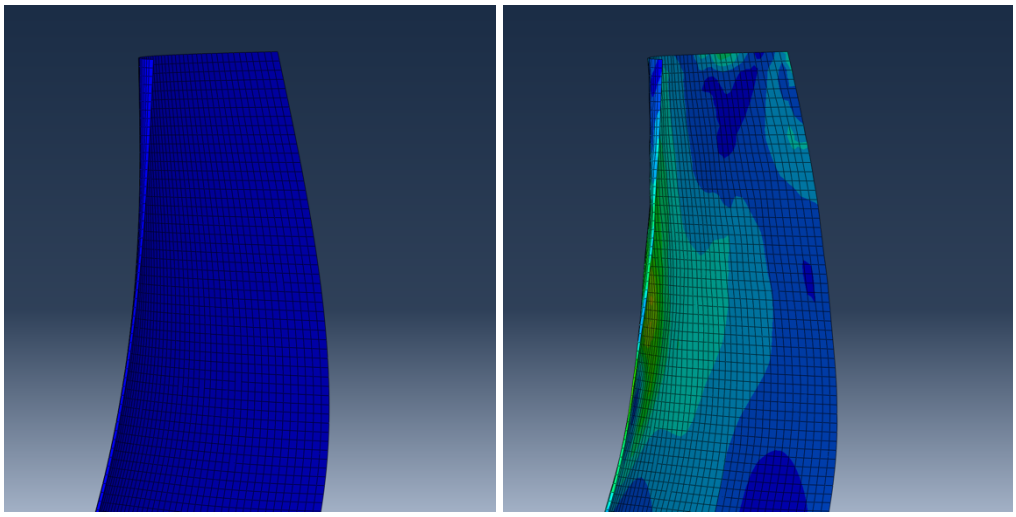

Node: P5-1.7554

	1	2	3	Magnitude
Base coordinates:	2.16540e+02,	1.19424e+03,	7.63574e+01,	-
Scale:	1.00000e+00,	1.00000e+00,	1.00000e+00,	-
Deformed coordinates (unscaled):	2.18921e+02,	1.19424e+03,	7.63574e+01,	-
Deformed coordinates (scaled):	2.18921e+02,	1.19424e+03,	7.63574e+01,	-
Displacement (unscaled):	2.38098e+00,	0.00000e+00,	0.00000e+00,	2.38098e+00

Figure 5.2 : ABAQUS output of maximum deformation at the impact at -5º

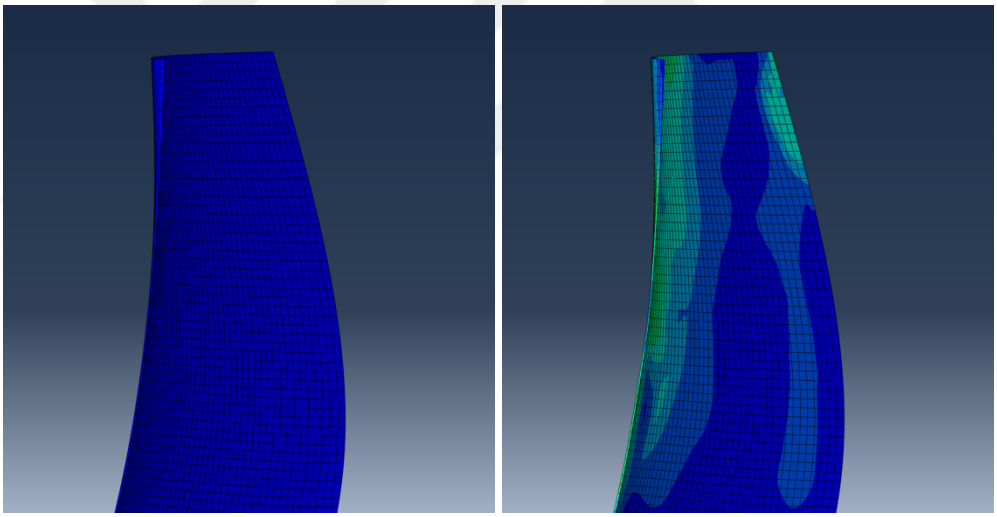

Node: BLADES-1.7602

	1	2	3	Magnitude
Base coordinates:	2.16547e+02,	1.19413e+03,	7.68930e+01,	-
Scale:	1.00000e+00,	1.00000e+00,	1.00000e+00,	-
Deformed coordinates (unscaled):	2.19821e+02,	1.19413e+03,	7.68930e+01,	-
Deformed coordinates (scaled):	2.19821e+02,	1.19413e+03,	7.68930e+01,	-
Displacement (unscaled):	3.27405e+00,	0.00000e+00,	0.00000e+00,	3.27405e+00

Figure 5.3 : ABAQUS output of maximum deformation at the impact at 0º

ABAQUS results represent at Figure 5.2 yeilds an increase in deformation with 2.38 mm on the initial impact location in the case of a 5º increase of the blade profile. In Figure 5.3 where the reference blade is subjected to the impact, showed the maximum amount of deformation of the section with 3.27 mm of bending damage.

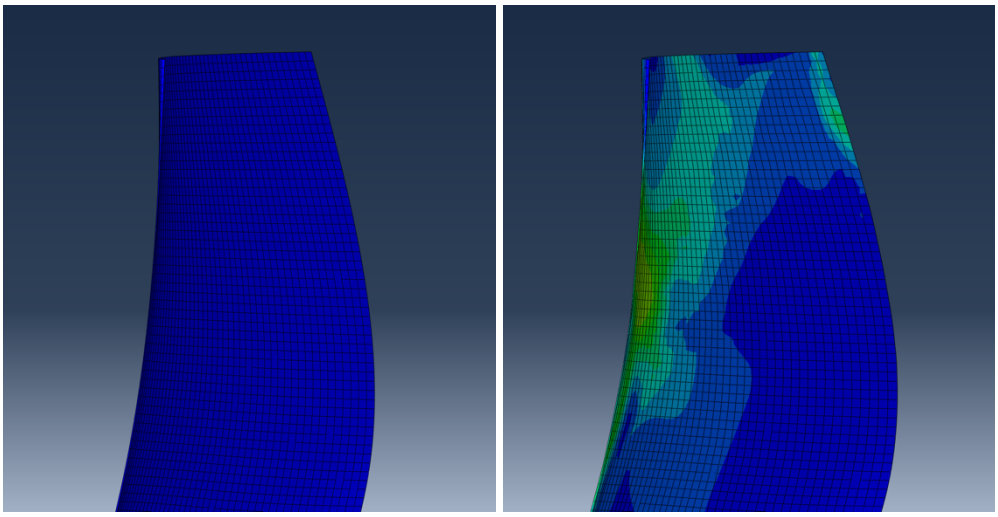

Node: M5-1.7554

	1	2	3	Magnitude
Base coordinates:	2.16547e+02,	1.19413e+03,	7.68930e+01,	-
Scale:	1.00000e+00,	1.00000e+00,	1.00000e+00,	-
Deformed coordinates (unscaled):	2.17959e+02,	1.19413e+03,	7.68930e+01,	-
Deformed coordinates (scaled):	2.17959e+02,	1.19413e+03,	7.68930e+01,	-
Displacement (unscaled):	1.41162e+00,	0.00000e+00,	0.00000e+00,	1.41162e+00

Figure 5.4 : ABAQUS output of maximum deformation at the impact at 5º

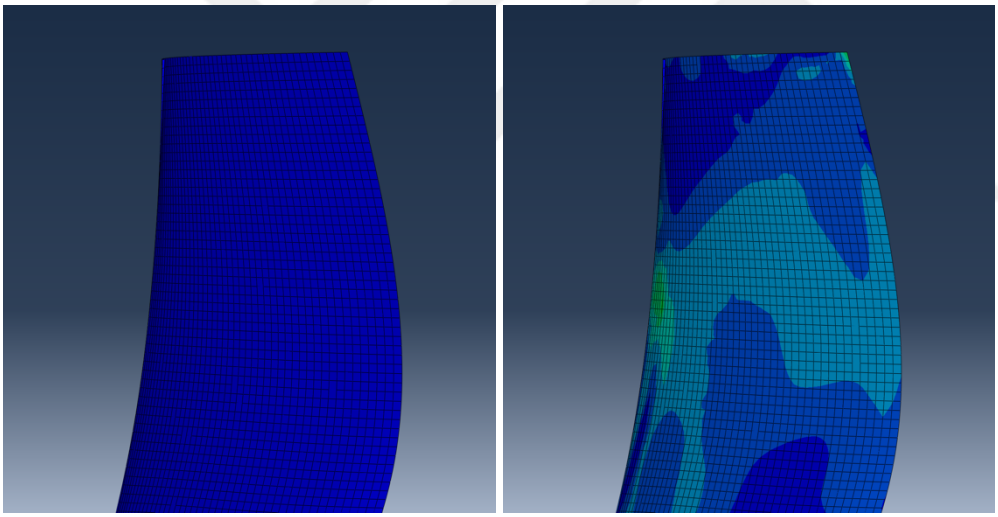

Node: M10-1.7554

	1	2	3	Magnitude
Base coordinates:	2.16458e+02,	1.19417e+03,	7.79943e+01,	-
Scale:	1.00000e+00,	1.00000e+00,	1.00000e+00,	-
Deformed coordinates (unscaled):	2.16790e+02,	1.19417e+03,	7.79943e+01,	-
Deformed coordinates (scaled):	2.16790e+02,	1.19417e+03,	7.79943e+01,	-
Displacement (unscaled):	3.32031e-01,	0.00000e+00,	0.00000e+00,	3.32031e-01

Figure 5.5 : ABAQUS output of maximum deformation at the impact at 10º

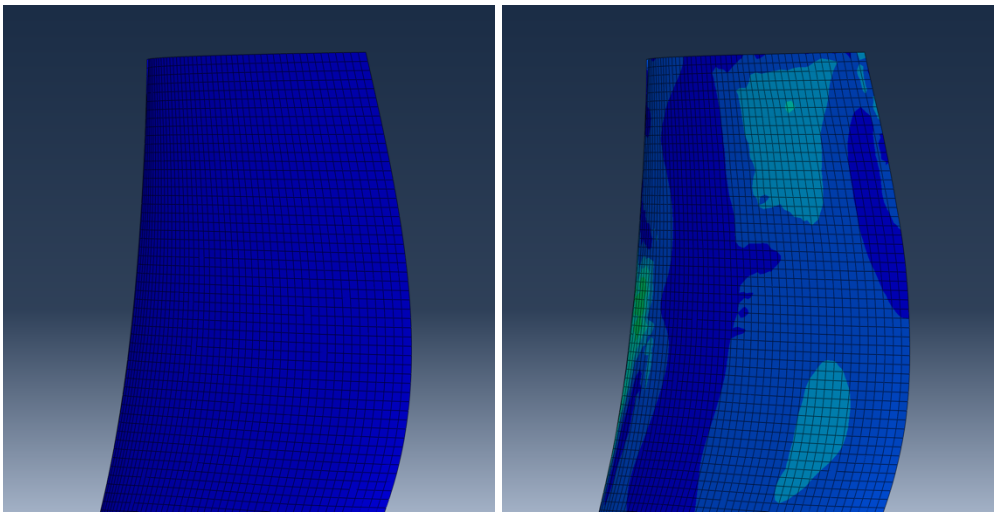

Node: M15-1.7554

	1	2	3	Magnitude
Base coordinates:	2.16547e+02,	1.19413e+03,	7.68929e+01,	–
Scale:	1.00000e+00,	1.00000e+00,	1.00000e+00,	–
Deformed coordinates (unscaled):	2.16800e+02,	1.19413e+03,	7.68929e+01,	–
Deformed coordinates (scaled):	2.16800e+02,	1.19413e+03,	7.68929e+01,	–
Displacement (unscaled):	2.52686e-01,	0.00000e+00,	0.00000e+00,	2.52686e-01

Figure 5.6 : ABAQUS output of maximum deformation at the impact at 15º

Between profile angles of 5º & 15º, a significant decrease in sustained damage was observed as shown in Figure 5.5, Figure 5.6 & Figure 5.7. At the profile angle of 5º, recorded damage was at 1.41 mm while at angles of 10º & 15º, the displacements were measured at 0.33 mm & 0.25 mm. 10º of profile angle also yielded the least amount of bending damage with a 1.8kg projectile.

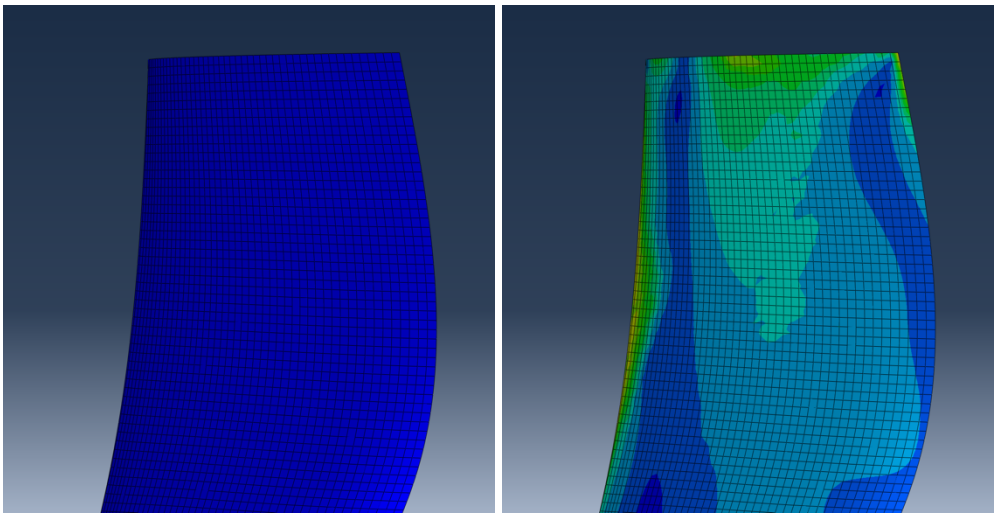

Node: M20-1.7554

	1	2	3	Magnitude
Base coordinates:	2.17000e+02,	1.19417e+03,	7.88047e+01,	–
Scale:	1.00000e+00,	1.00000e+00,	1.00000e+00,	–
Deformed coordinates (unscaled):	2.16302e+02,	1.19417e+03,	7.88047e+01,	–
Deformed coordinates (scaled):	2.16302e+02,	1.19417e+03,	7.88047e+01,	–
Displacement (unscaled):	-6.97601e-01,	0.00000e+00,	0.00000e+00,	6.97601e-01

Figure 5.7 : ABAQUS output of maximum deformation at the impact at 20º

At the profile angle of 20º, the trend of decreasing sustained damage halts as shown in Figure 5.7, maximum nodal displacement is recorded as 0.69 mm. Analysis results indicate that rotating the profile at 80% height of the reference fan blade design which is set at 0º yielded significant improvements in terms of the maximum allowed bending distance until profile angle of 15º.

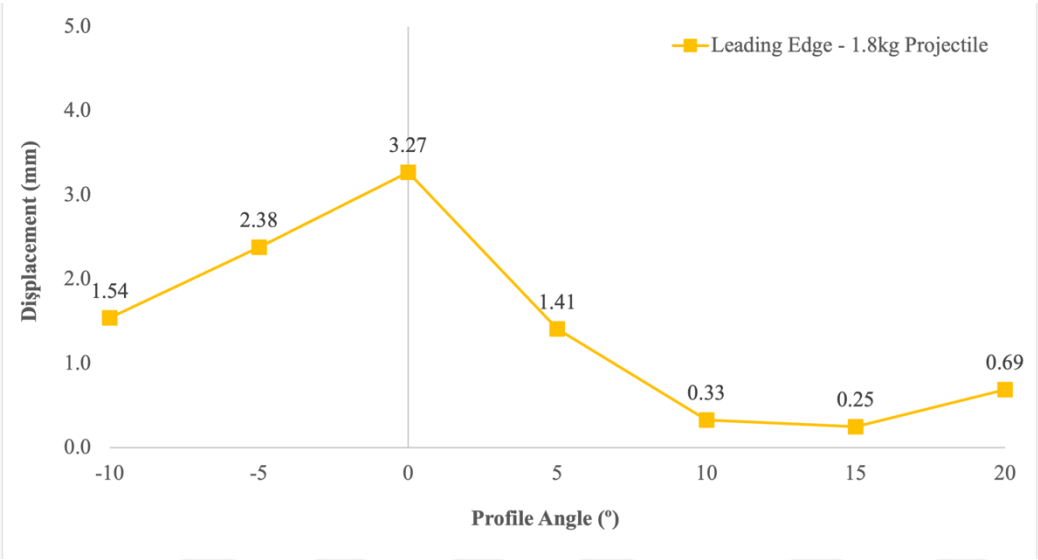

Figure 5.8 : Maximum nodal displacement to profile angle graph for 1.8kg weighted projectile at the leading edge of the blade.

5.2 Bending at the Leading Edge of the Fan Blade with a 3.6 kg projectile

Different from the analyses mentioned in Section 5.1, an impact scenario where a 3.6 kg projectile hits a fan blade at the leading-edge section is investigated. Figures from 5.9 to 5.15 represent the visuals of the blade before and after each impact simulation as well as the ABAQUS outputs featuring the displacement of the node which sustained the most plastic deformation in relation to its original position. Profile angle to nodal displacement graph is shown in Figure 5.16.

The initial analysis result yielded 18.57 mm of bending damage at -10º profile angle as shown in Figure 5.9. The recorded damage significantly increased in simulations with 3.6 kg projectile due to the usage of a heavier bird model.

The trajectory of increasing damage is sustained until 5º of profile angle. At -5º, the damage is recorded as 20.88 mm as shown in Figure 5.10, while at 0º & 5º the recorded maximum nodal displacement is 23.27 mm & 22.96 mm as presented in Figures 5.11 & Figure 5.12. At the profile angle of 0º, the maximum amount of nodal displacement is observed with the usage of 3.6 kg projectile, similar to the simulations with 1.8 kg projectile.

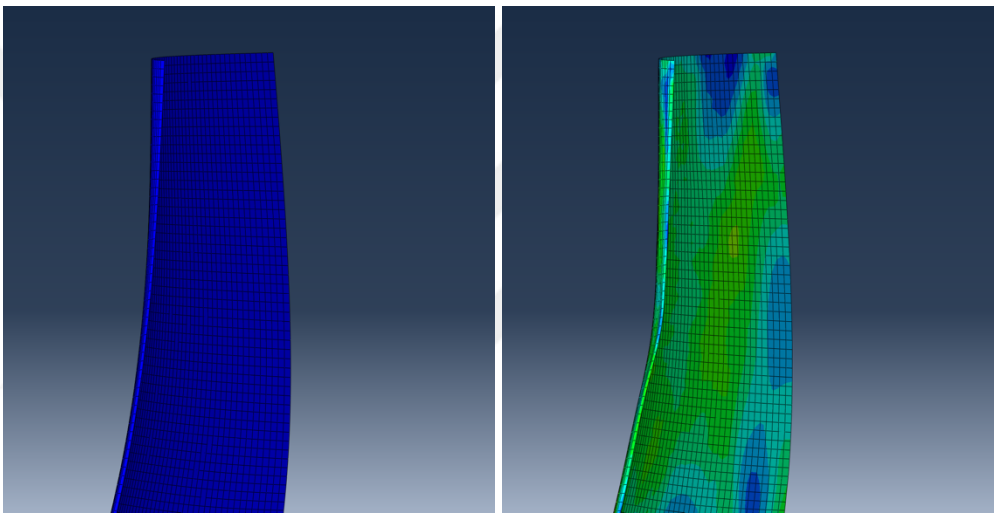

Node: P10-1.7602

	1	2	3	Magnitude
Base coordinates:	2.16529e+02,	1.19420e+03,	7.65364e+01,	-
Scale:	1.00000e+00,	1.00000e+00,	1.00000e+00,	-
Deformed coordinates (unscaled):	2.35101e+02,	1.19420e+03,	7.65364e+01,	-
Deformed coordinates (scaled):	2.35101e+02,	1.19420e+03,	7.65364e+01,	-
Displacement (unscaled):	1.85720e+01,	0.00000e+00,	0.00000e+00,	1.85720e+01

Figure 5.9 : ABAQUS output of maximum deformation at the impact at -10º

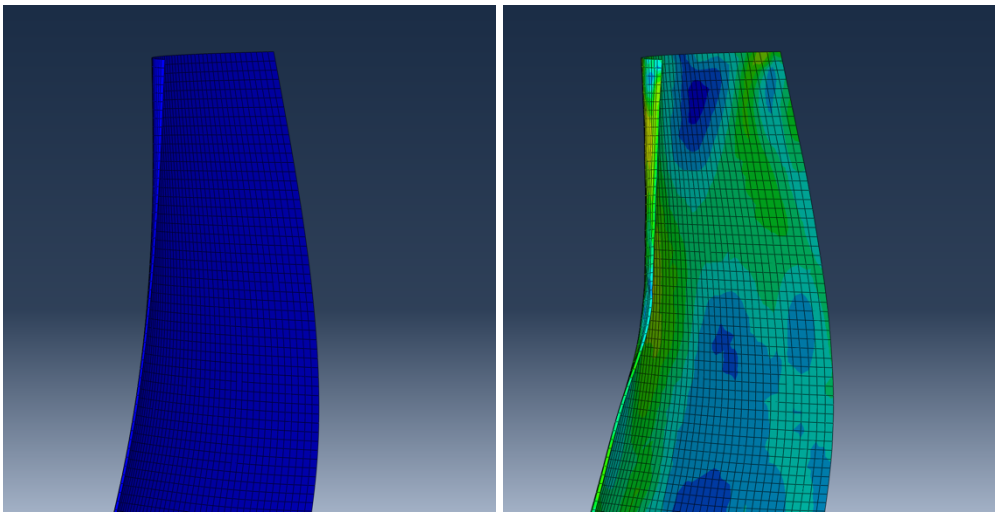

Node: P5-1.7554

	1	2	3	Magnitude
Base coordinates:	2.16540e+02,	1.19424e+03,	7.63574e+01,	–
Scale:	1.00000e+00,	1.00000e+00,	1.00000e+00,	–
Deformed coordinates (unscaled):	2.37425e+02,	1.19424e+03,	7.63574e+01,	–
Deformed coordinates (scaled):	2.37425e+02,	1.19424e+03,	7.63574e+01,	–
Displacement (unscaled):	2.08848e+01,	0.00000e+00,	0.00000e+00,	2.08848e+01

Figure 5.10 : ABAQUS output of maximum deformation at the impact at -5º

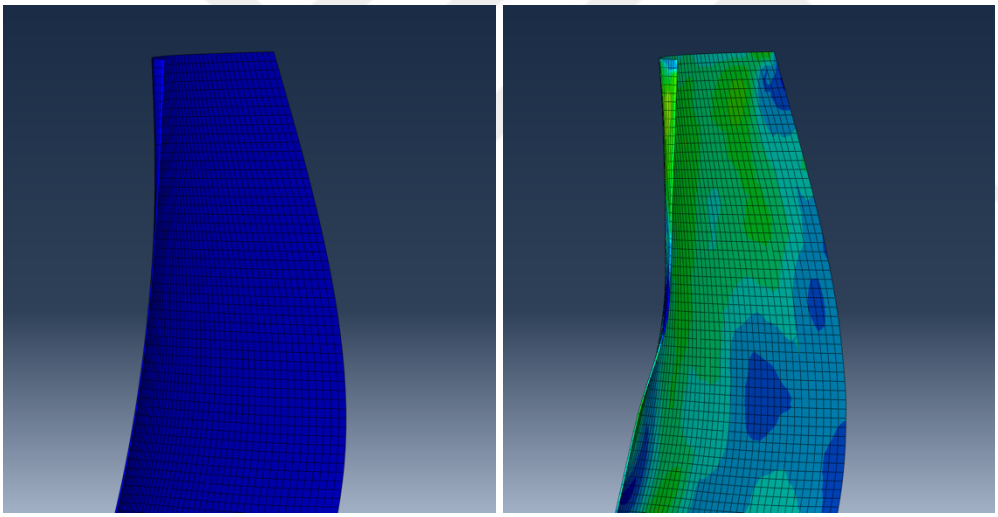

Node: BLADES-1.7602

	1	2	3	Magnitude
Base coordinates:	2.16547e+02,	1.19413e+03,	7.68930e+01,	–
Scale:	1.00000e+00,	1.00000e+00,	1.00000e+00,	–
Deformed coordinates (unscaled):	2.39823e+02,	1.19413e+03,	7.68930e+01,	–
Deformed coordinates (scaled):	2.39823e+02,	1.19413e+03,	7.68930e+01,	–
Displacement (unscaled):	2.32764e+01,	0.00000e+00,	0.00000e+00,	2.32764e+01

Figure 5.11 : ABAQUS output of maximum deformation at the impact at 0º

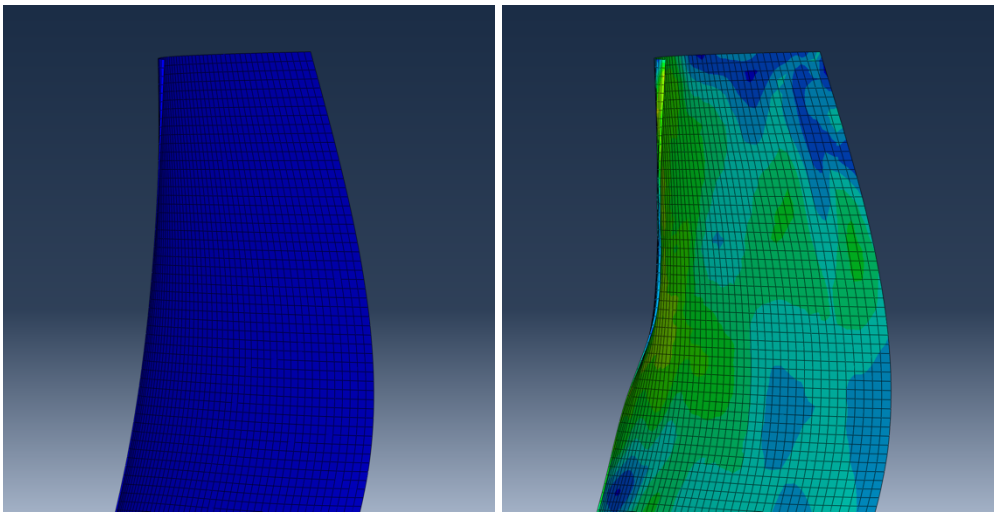

Node: M5-1.7554

	1	2	3	Magnitude
Base coordinates:	2.16547e+02,	1.19413e+03,	7.68930e+01,	–
Scale:	1.00000e+00,	1.00000e+00,	1.00000e+00,	–
Deformed coordinates (unscaled):	2.39514e+02,	1.19413e+03,	7.68930e+01,	–
Deformed coordinates (scaled):	2.39514e+02,	1.19413e+03,	7.68930e+01,	–
Displacement (unscaled):	2.29675e+01,	0.00000e+00,	0.00000e+00,	2.29675e+01

Figure 5.12 : ABAQUS output of maximum deformation at the impact at 5º

At the profile angle of 10º, a significant decrease in sustained damage is observed. Figure 5.13 indicates that bending damage of 9.55 mm is present while at 15º & 20º the recorded maximum nodal displacement is 6.87 mm & 4.57 mm as presented in Figures 5.14 & Figure 5.15.

Different to the simulations with 1.8 kg projectile, the damage recorded at the 20º profile angle keeps decreasing trajectory instead of yielding an increased amount of displacement.

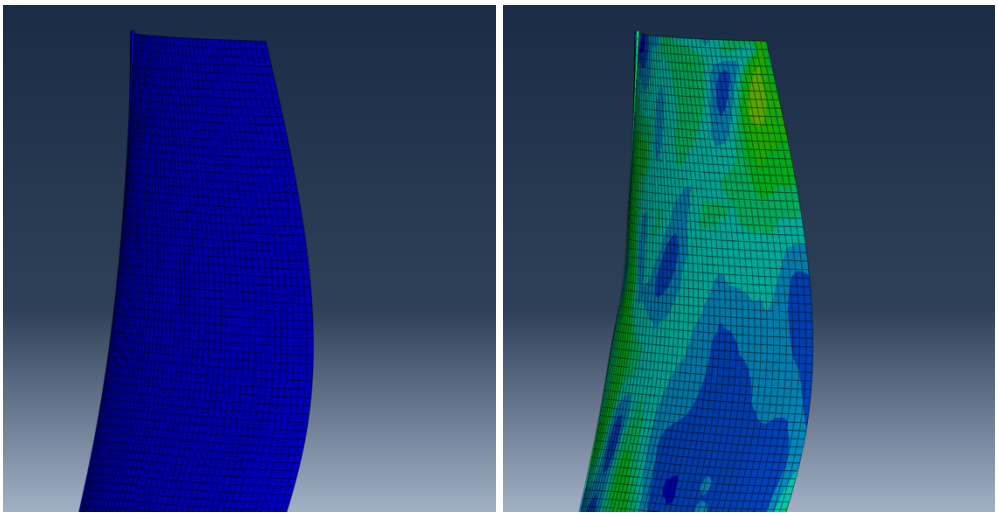

Node: M10-1.7554

	1	2	3	Magnitude
Base coordinates:	2.16458e+02,	1.19417e+03,	7.79943e+01,	-
Scale:	1.00000e+00,	1.00000e+00,	1.00000e+00,	-
Deformed coordinates (unscaled):	2.26011e+02,	1.19417e+03,	7.79943e+01,	-
Deformed coordinates (scaled):	2.26011e+02,	1.19417e+03,	7.79943e+01,	-
Displacement (unscaled):	9.55215e+00,	0.00000e+00,	0.00000e+00,	9.55215e+00

Figure 5.13 : ABAQUS output of maximum deformation at the impact at 10º

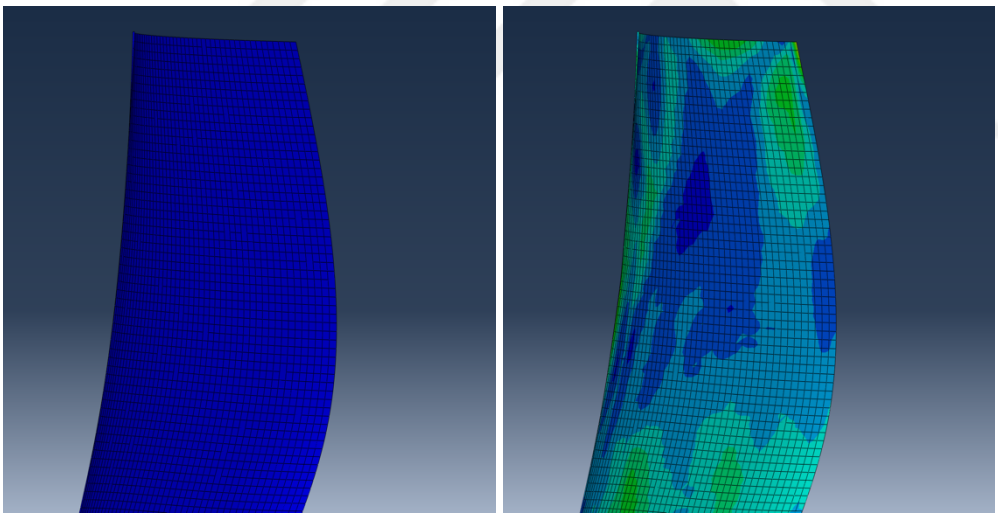

Node: M15-1.7554

	1	2	3	Magnitude
Base coordinates:	2.16547e+02,	1.19413e+03,	7.68929e+01,	-
Scale:	1.00000e+00,	1.00000e+00,	1.00000e+00,	-
Deformed coordinates (unscaled):	2.23420e+02,	1.19413e+03,	7.68929e+01,	-
Deformed coordinates (scaled):	2.23420e+02,	1.19413e+03,	7.68929e+01,	-
Displacement (unscaled):	6.87337e+00,	0.00000e+00,	0.00000e+00,	6.87337e+00

Figure 5.14 : ABAQUS output of maximum deformation at the impact at 15º

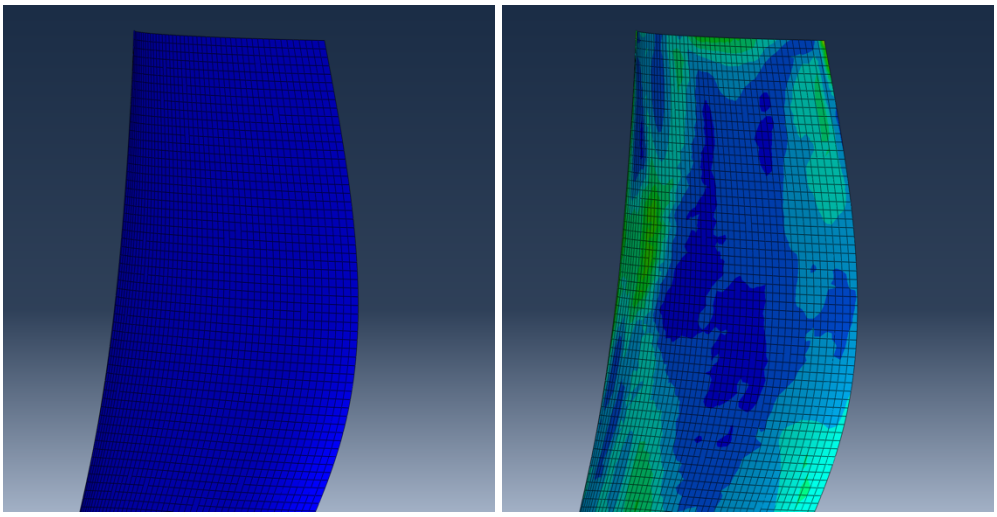

Node: M20-1.7554

	1	2	3	Magnitude
Base coordinates:	2.17000e+02,	1.19417e+03,	7.88047e+01,	–
Scale:	1.00000e+00,	1.00000e+00,	1.00000e+00,	–
Deformed coordinates (unscaled):	2.21522e+02,	1.19417e+03,	7.88047e+01,	–
Deformed coordinates (scaled):	2.21522e+02,	1.19417e+03,	7.88047e+01,	–
Displacement (unscaled):	4.52295e+00,	0.00000e+00,	0.00000e+00,	4.52295e+00

Figure 5.15 : ABAQUS output of maximum deformation at the impact at 20º

Analysis results are fairly similar to the previous simulation with a 1.8kg projectile. Deformation characteristic at the leading edge of the blade massively improved between a profile angle of 10º & 20º and worsened between -10º and 0º as shown in Figure 5.16.

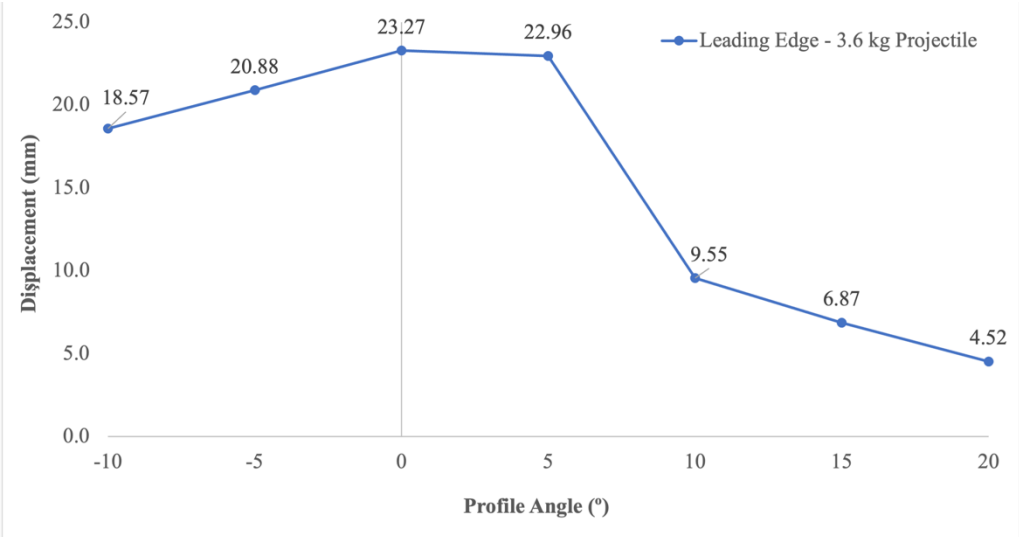

Figure 5.16 : Maximum nodal displacement to profile angle graph for 3.6 kg weighted projectile at the leading edge of the blade

5.3 Denting at the Middle Section of the Blade with a 1.8 kg Projectile

In order to investigate the denting effect after a bird strike, projectiles weighted at 1.8 kg were struck against a fan blade at the middle section. Initial simulations at the middle section with a 1.8kg projectile yielded 1.41 mm of damage at -10º, followed by a measured displacement of 1.25 mm at -5º. The most amount of sustained damage was observed at 2.47 mm at the 0º profile angle different to the simulations where 1.8 kg projectiles are used. At 5º profile angle, measured maximum nodal displacement decreased to 0.42 mm while keeping a relatively steady trajectory between 5º & 20º of profile angles with 0.61 mm, 0.31mm & 0.75 mm of nodal displacement at 10º, 15º & 20º angles respectively. ABAQUS outputs of the related simulations is shown at Figure 5.18 while the profile angle to nodal displacement graph is presented in Figure 5.17.

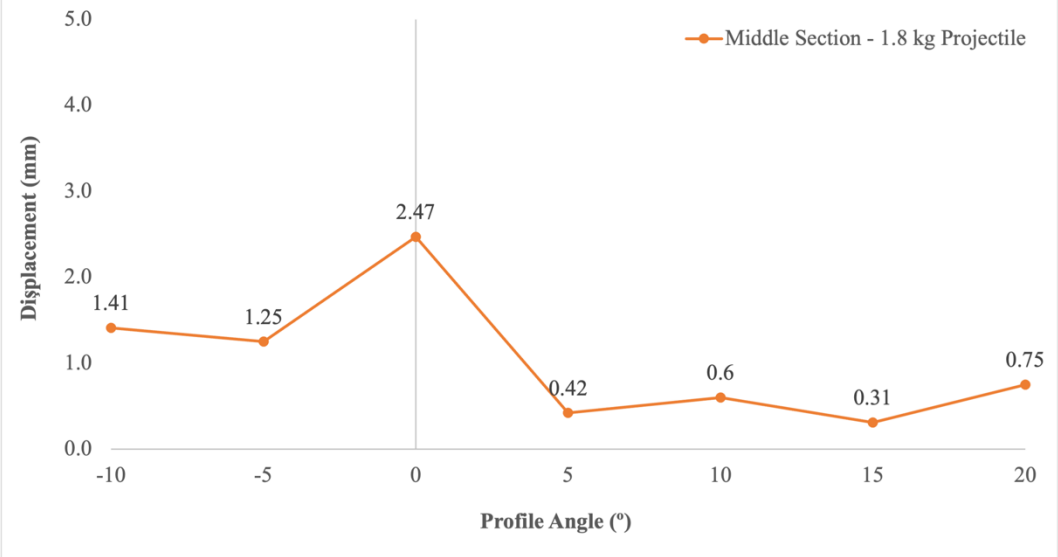

Figure 5.17 : Maximum nodal displacement to profile angle graph for 1.8 kg weighted projectile at the middle section of the blade

Strike simulations aiming for understanding the damage characteristics near the center of the blade with a 1.8 kg projectile suggest that plastic deformations are minimized between 5º & 15º profile angles.

Node: P10-1.5695 Profile Angle: -10º

	1	2	3	Magnitude
Base coordinates:	2.02571e+02,	1.19788e+03,	-5.05796e+01,	-
Scale:	1.00000e+00,	1.00000e+00,	1.00000e+00,	-
Deformed coordinates (unscaled):	2.03980e+02,	1.19785e+03,	-5.05291e+01,	-
Deformed coordinates (scaled):	2.03980e+02,	1.19785e+03,	-5.05291e+01,	-
Displacement (unscaled):	1.40942e+00,	-2.93579e-02,	5.04456e-02,	1.41063e+00

Node: P5-1.5659 Profile Angle: -5º

	1	2	3	Magnitude
Base coordinates:	2.10812e+02,	1.19779e+03,	-4.77996e+01,	-
Scale:	1.00000e+00,	1.00000e+00,	1.00000e+00,	-
Deformed coordinates (unscaled):	2.12064e+02,	1.19783e+03,	-4.77570e+01,	-
Deformed coordinates (scaled):	2.12064e+02,	1.19783e+03,	-4.77570e+01,	-
Displacement (unscaled):	1.25232e+00,	3.98254e-02,	4.26025e-02,	1.25368e+00

Node: BLADES-1.5536 Profile Angle: 0º

	1	2	3	Magnitude
Base coordinates:	2.20644e+02,	1.19876e+03,	-5.41142e+01,	-
Scale:	1.00000e+00,	1.00000e+00,	1.00000e+00,	-
Deformed coordinates (unscaled):	2.23118e+02,	1.19872e+03,	-5.40643e+01,	-
Deformed coordinates (scaled):	2.23118e+02,	1.19872e+03,	-5.40643e+01,	-
Displacement (unscaled):	2.47431e+00,	-3.82591e-02,	4.98912e-02,	2.47511e+00

Node: M5-1.5501 Profile Angle: 5º

	1	2	3	Magnitude
Base coordinates:	2.32586e+02,	1.19870e+03,	-5.22673e+01,	-
Scale:	1.00000e+00,	1.00000e+00,	1.00000e+00,	-
Deformed coordinates (unscaled):	2.33004e+02,	1.19873e+03,	-5.21967e+01,	-
Deformed coordinates (scaled):	2.33004e+02,	1.19873e+03,	-5.21967e+01,	-
Displacement (unscaled):	4.17603e-01,	3.07922e-02,	7.05566e-02,	4.24639e-01

Node: M10-1.5501 Profile Angle: 10º

	1	2	3	Magnitude
Base coordinates:	2.44116e+02,	1.19865e+03,	-4.82843e+01,	-
Scale:	1.00000e+00,	1.00000e+00,	1.00000e+00,	-
Deformed coordinates (unscaled):	2.44715e+02,	1.19862e+03,	-4.83223e+01,	-
Deformed coordinates (scaled):	2.44715e+02,	1.19862e+03,	-4.83223e+01,	-
Displacement (unscaled):	5.99121e-01,	-3.75977e-02,	-3.79639e-02,	6.01499e-01

Node: M15-1.5659 Profile Angle: 15º

	1	2	3	Magnitude
Base coordinates:	2.50955e+02,	1.19885e+03,	-3.61448e+01,	-
Scale:	1.00000e+00,	1.00000e+00,	1.00000e+00,	-
Deformed coordinates (unscaled):	2.51235e+02,	1.19881e+03,	-3.60269e+01,	-
Deformed coordinates (scaled):	2.51235e+02,	1.19881e+03,	-3.60269e+01,	-
Displacement (unscaled):	2.79602e-01,	-4.64020e-02,	1.17981e-01,	3.07002e-01

Node: M20-1.5343 Profile Angle: 20º

	1	2	3	Magnitude
Base coordinates:	2.72047e+02,	1.19793e+03,	-4.76604e+01,	-
Scale:	1.00000e+00,	1.00000e+00,	1.00000e+00,	-
Deformed coordinates (unscaled):	2.72772e+02,	1.19788e+03,	-4.74617e+01,	-
Deformed coordinates (scaled):	2.72772e+02,	1.19788e+03,	-4.74617e+01,	-
Displacement (unscaled):	7.25830e-01,	-5.49927e-02,	1.98730e-01,	7.54551e-01

Figure 5.18 : ABAQUS output of maximum deformation at the impact at 20º

5.4 Denting at the Middle Section of the Blade with a 3.6 kg Projectile

Similar to the Section 5.3, projectiles weighted at 3.6 kg were struck against a fan blade in the middle section. Initial simulations at the middle section with a 3.6 kg projectile yielded 17.87 mm of damage at -10º, followed by a slightly decreasing measured displacement of 16.69 mm at -5º and 15.45 mm at 0º. The most amount of sustained damage was observed at 17.87 mm at the -10º profile angle different from the simulations where 1.8 kg projectiles are used. At the 5º profile angle, measured maximum nodal displacement decreased to 11.21 mm while keeping a relatively steady trajectory between 5º & 15º profile angles with 11.21 mm, 11.61 mm & 10.96 mm of nodal displacement at 5º, 10º & 15º angles respectively. At 20º, measured sustained damage slightly dropped to 9.46 mm. Profile angle to nodal displacement graph is presented in Figure 5.19 as well as the ABAQUS outputs of the related simulations are shown at Figure 5.20.

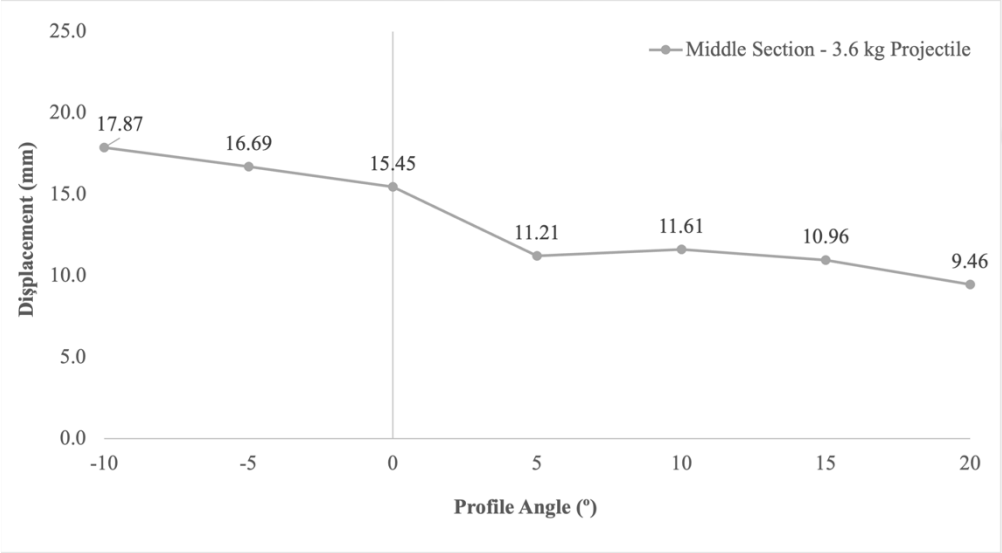

Figure 5.19 : Maximum nodal displacement to profile angle graph for 3.6 kg weighted projectile at the leading edge of the blade

Weight increase from 1.8 kg to 3.6 kg validates the deformation behavior of the previous analysis results. Deformation characteristic at the leading edge of the blade shows significant improvements between a profile angle of 5º & 20º. Reduction of angle below 0º slightly increases the measured deformation and indicates is not a viable design choice.

Node: P10-1.5695 Profile Angle: -10º

	1	2	3	Magnitude
Base coordinates:	2.02571e+02,	1.19788e+03,	-5.05796e+01,	-
Scale:	1.00000e+00,	1.00000e+00,	1.00000e+00,	-
Deformed coordinates (unscaled):	2.20425e+02,	1.19695e+03,	-5.03860e+01,	-
Deformed coordinates (scaled):	2.20425e+02,	1.19695e+03,	-5.03860e+01,	-
Displacement (unscaled):	1.78541e+01,	-9.27878e-01,	1.93553e-01,	1.78793e+01

Node: P5-1.5659 Profile Angle: -5º

	1	2	3	Magnitude
Base coordinates:	2.10812e+02,	1.19779e+03,	-4.77996e+01,	-
Scale:	1.00000e+00,	1.00000e+00,	1.00000e+00,	-
Deformed coordinates (unscaled):	2.27477e+02,	1.19696e+03,	-4.72633e+01,	-
Deformed coordinates (scaled):	2.27477e+02,	1.19696e+03,	-4.72633e+01,	-
Displacement (unscaled):	1.66652e+01,	-8.37769e-01,	5.36377e-01,	1.66948e+01

Node: BLADES-1.5536 Profile Angle: 0º

	1	2	3	Magnitude
Base coordinates:	2.20644e+02,	1.19876e+03,	-5.41142e+01,	-
Scale:	1.00000e+00,	1.00000e+00,	1.00000e+00,	-
Deformed coordinates (unscaled):	2.36042e+02,	1.19797e+03,	-5.30356e+01,	-
Deformed coordinates (scaled):	2.36042e+02,	1.19797e+03,	-5.30356e+01,	-
Displacement (unscaled):	1.53983e+01,	-7.90372e-01,	1.07863e+00,	1.54563e+01

Node: M5-1.5501 Profile Angle: 5º

	1	2	3	Magnitude
Base coordinates:	2.32586e+02,	1.19870e+03,	-5.22673e+01,	-
Scale:	1.00000e+00,	1.00000e+00,	1.00000e+00,	-
Deformed coordinates (unscaled):	2.43584e+02,	1.19768e+03,	-5.03226e+01,	-
Deformed coordinates (scaled):	2.43584e+02,	1.19768e+03,	-5.03226e+01,	-
Displacement (unscaled):	1.09974e+01,	-1.01746e+00,	1.94470e+00,	1.12143e+01

Node: M10-1.5501 Profile Angle: 10º

	1	2	3	Magnitude
Base coordinates:	2.44116e+02,	1.19865e+03,	-4.82843e+01,	-
Scale:	1.00000e+00,	1.00000e+00,	1.00000e+00,	-
Deformed coordinates (unscaled):	2.54998e+02,	1.19741e+03,	-4.44086e+01,	-
Deformed coordinates (scaled):	2.54998e+02,	1.19741e+03,	-4.44086e+01,	-
Displacement (unscaled):	1.08826e+01,	-1.24753e+00,	3.87573e+00,	1.16193e+01

Node: M15-1.5659 Profile Angle: 15º

	1	2	3	Magnitude
Base coordinates:	2.50955e+02,	1.19885e+03,	-3.61448e+01,	-
Scale:	1.00000e+00,	1.00000e+00,	1.00000e+00,	-
Deformed coordinates (unscaled):	2.60629e+02,	1.19747e+03,	-3.11690e+01,	-
Deformed coordinates (scaled):	2.60629e+02,	1.19747e+03,	-3.11690e+01,	-
Displacement (unscaled):	9.67358e+00,	-1.38730e+00,	4.97583e+00,	1.09664e+01

Node: M20-1.5343 Profile Angle: 20º

	1	2	3	Magnitude
Base coordinates:	2.60087e+02,	1.19807e+03,	-5.48367e+01,	-
Scale:	1.00000e+00,	1.00000e+00,	1.00000e+00,	-
Deformed coordinates (unscaled):	2.68343e+02,	1.19694e+03,	-5.03586e+01,	-
Deformed coordinates (scaled):	2.68343e+02,	1.19694e+03,	-5.03586e+01,	-
Displacement (unscaled):	8.25659e+00,	-1.12936e+00,	4.47809e+00,	9.46045e+00

Figure 5.20 : ABAQUS output of maximum deformation at the impact at 20º

5.5 Ultimate Tensile Strength

To validate the material failure aspect of the simulations, the analyses where 3.6 kg projectiles were constructed at the middle section and the leading edge of the fan blade at the reference angle are observed in terms of maximum stress since the simulations with 3.6 kg projectiles yielded the most amount of nodal displacement. Stress values measured at the impact location for both leading edge and middle sections are presented in Figure 5.21 & Figure 5.22. Stress values when a 3.6 kg projectile struck at the leading edge peaked at 736 MPa while dropping between 250 MPa – 400 MPa

during a period where vibrations from the initial impact are not dissipated. The middle section simulation yields a maximum stress value of 629 MPa while settling between 250 MPa – 350 MPa.

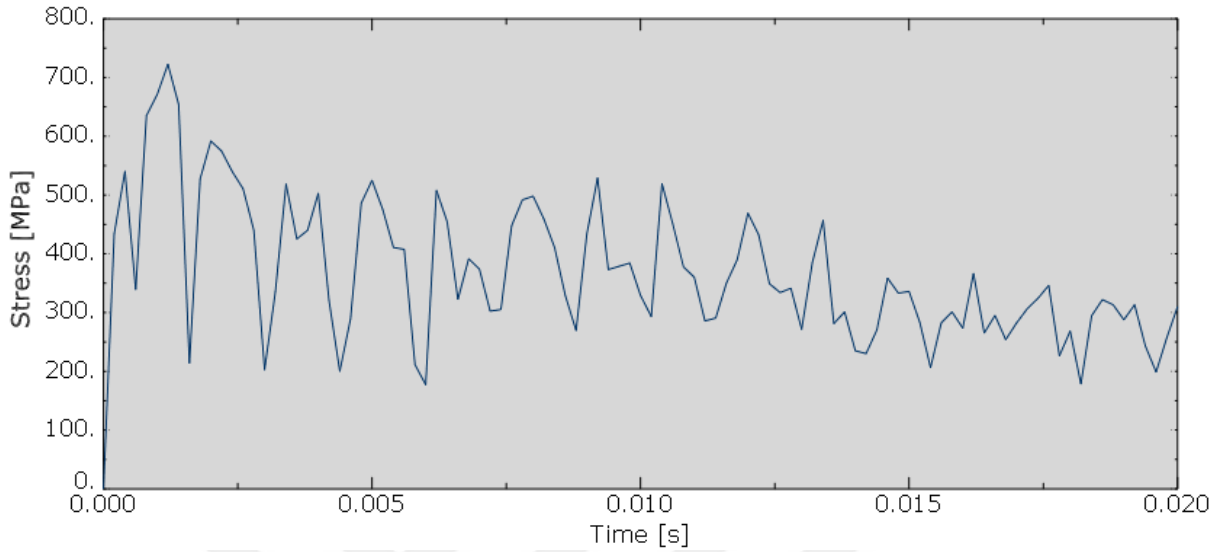

Figure 5.21 : Maximum stress to time graph for 3.6 kg weighted projectile at the leading edge of the blade.

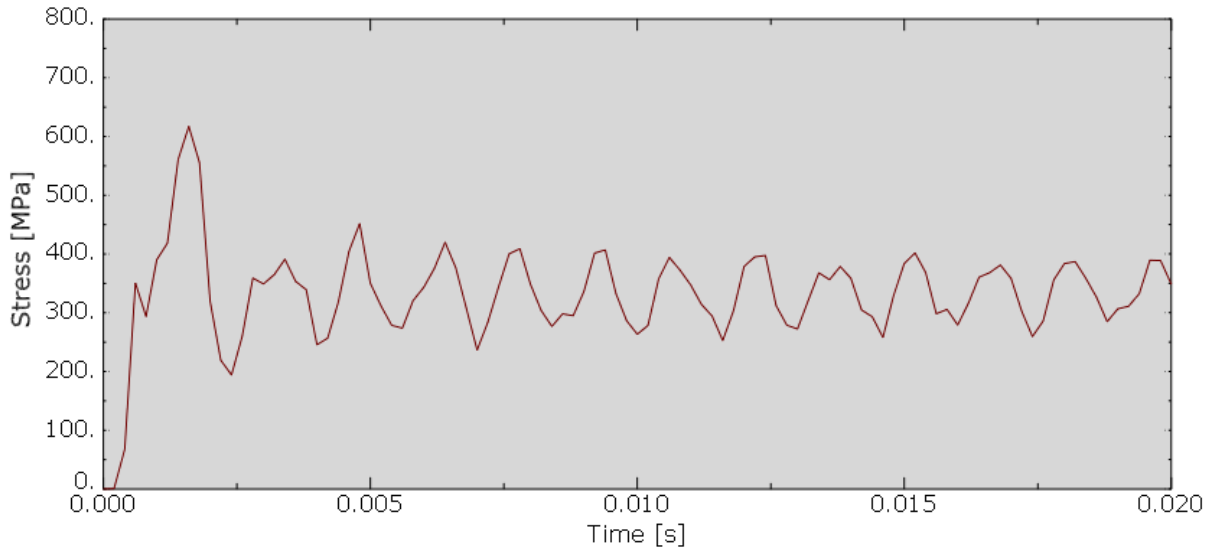

Figure 5.22 : Maximum stress to time graph for 3.6 kg weighted projectile at the middle section of the blade.

Stress behavior and the maximum stress values obtained from the analyses rule out any tear and crack damage to be potentially occurred since the maximum stress observed stays below the ultimate tensile stress value of the fan blade material which is at 970 MPa [30].

CONCLUSION & DISCUSSION

The general purpose of the study is to improve the deformation characteristics of the fan blade in a bird strike event. In order to set up an analysis environment similar to real-life occurrences, previous reports from aviation authorities were examined and a portion of impact parameters were determined. As a result, 2 different bird models with 2 different dimensions were used as projectiles and 7 different fan blade models were created.

Simulations focusing on leading edge damage indicated that increasing the profile angle at 80% height of the blade yields significant improvements in terms of plastic deformation endurance. Considering the fact that allowable tolerances at the surface of the fan blades are generally defined by fractions of a millimeter, improvements in deformation durability mean significant financial gains for both engine manufacturers and airline operators.

Due to not having access to a practical test environment and the cost of manufacturing a sample blade being financially unattainable, impact tests are limited to a simulation environment. In addition, the probable aerodynamic effect of altering the blade geometry is not within the scope of this study and may be researched in future works on a similar subject.

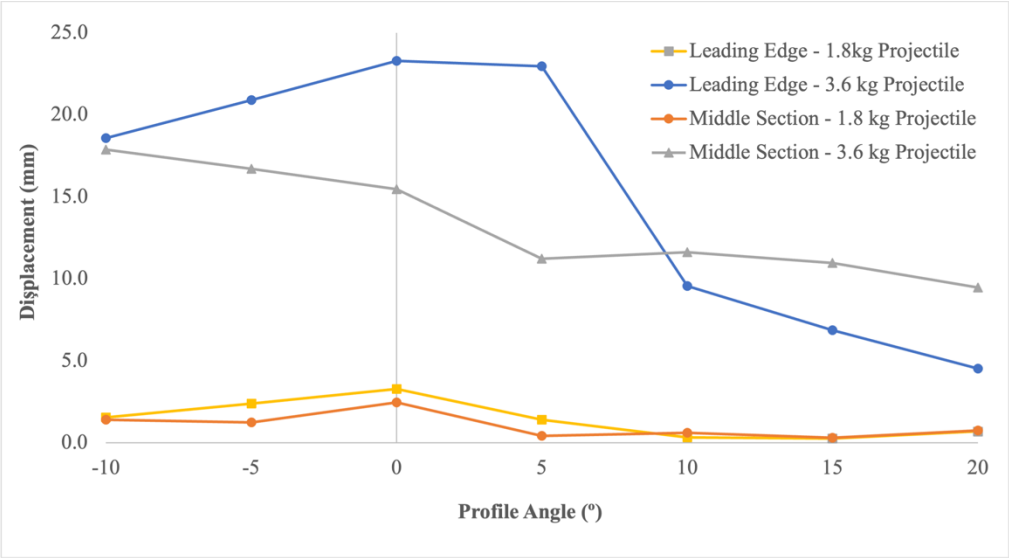

Figure 6.1 : Maximum nodal displacement to profile angle graph for all simulations.

REFERENCES

[1] Gudmundsson, S. (2022). *Thrust modeling for gas turbines.* General Aviation Aircraft Design, 573–595.

[2] Taylor, Z. J., Palombi, E., Gurka, R., & Kopp, G. A. (2011). *Features of the turbulent flow around symmetric elongated bluff bodies.* Journal of Fluids and Structures, 27(2), 250–265.

[3] Metz, I., Ellerbroek, J., Mühlhausen, T., Kügler, D., Kern, S., & Hoekstra, J. (2021). *The efficacy of Operational Bird Strike Prevention*. Aerospace, 8(1), 17.

[4] Ćwiklak, J., Kobiałka, E., Goś, A. (2022). Experimental and numerical investigations of bird models for bird strike analysis. Energies, 15(10), 3699.

[5] Metz, I. C., Ellerbroek, J., Mühlhausen, T., Kügler, D., & Hoekstra, J. M. (2020). The bird strike challenge. Aerospace, 7(3), 26.

[6] Edge C.H, & Degrieck J. (1999). "Derivation of a Dummy Bird for Analysis and Test of Airframe structures," Farnborough Aerospace Centre, Hampshire, UK and Department of Applied Mechanics, University of Gent, Belgium, Technical Paper.

[7] Budgey, R. (2000). "The Development of a Substitute Artificial Bird by The International Birdstrike Research Group for use in Aircraft Component Testing," Birdstrike Avoidance Team, Central Science Laboratory.

[8] Goyal, V., Huertas, C., Leutwiler, T., Borrero, J., & Vasko, T. (2006). Robust bird-strike modeling based on SPH formulation using LS-Dyna. 47th AIAA/ASME/ASCE/AHS/ASC Structures, Structural Dynamics, and Materials Conference 14th AIAA/ASME/AHS Adaptive Structures Conference 7th.

[9] Mao, R. H., Meguid, S. A., Ng, T. Y. (2009). Effects of incidence angle in bird strike on integrity of aero-engine fan blade. International Journal of Crashworthiness, 14(4), 295–308.

[10] Upadhyay, R., & Sinha, S. (2018). *GE-90 and derivative fan blade manufacturing design*. Comprehensive Composite Materials II, 180–188.

[11] Steinegger, R. (2017). *Fuel economy as function of weight and distance*. Zürcher Fachhochschule.

[12] Heidari, M., Carlson, D., Sinha, S., Sadeghi, R., Heydari, C., Bayoumi, H., Son, J. (2008). An efficient multi-disciplinary simulation of engine fan-blade out event using MD NASTRAN. 49th AIAA/ASME/ASCE/AHS/ASC Structures, Structural Dynamics, and Materials Conferen

[13] Siddens, A.; Bayandor, J. (2011). *An extensive crashworthiness methodology for advanced propulsion systems, part II: Damage and vibration instability analysis of jet engine forward sections.* 49th AIAA Aerospace Sciences Meeting Including the New Horizons Forum and Aerospace Exposition.

[14] Karabacak, M., & Turan, O. (2019). *Turbofan engine weight estimation for preliminary design.* International Journal of Sustainable Aviation, 5(2), 87.

[15] Liu, Z., Chen, Z., & Chen, J. (2018). *The strength analysis of CFM56 engine blade*. MATEC Web of Conferences, 166, 04001.

[16] Zerbst, U., Madia, M., Klinger, C., Bettge, D., & Murakami, Y. (2019). *Defects as a root cause of fatigue failure of metallic components. III: Cavities, dents, corrosion pits, scratches*. Engineering Failure Analysis, 97, 759–776.

[17] European Aviation Safety Agency (2009). Bird Strike Damage & Windshield Bird Strike Final Report.

[18] Marulo, F., & Guida, M. (2014). Design criteria for birdstrike damage on windshield. Advances in Aircraft and Spacecraft Science, 1(2), 233–251.

[19] Kumar Jha, A., Sathyamoorthy, S., & Prakash, V. (2019). Bird strike damage and analysis of UAV's airframe. Procedia Structural Integrity, 14, 416–428.

[20] Shimamura, K., Shibue, T., & Grosch, D. J. (2004). *Numerical simulation of bird strike damage on Jet Engine Fan blade*. Emerging Technology in Fluids, Structures, and Fluid Structure Interactions: Volume 1, Fluid Dynamics and Fluid Structure Interactions.

[21] Vijay Sekar, K. S., & Pradeep Kumar, M. (2011). Finite element simulations of Ti6Al4V titanium alloy machining to assess material model parameters of the Johnson-cook constitutive equation. Journal of the Brazilian Society of Mechanical Sciences and Engineering, 33(2), 203–211.

[22] Wang, F. S., & Yue, Z. F. (2010). *Numerical simulation of damage and failure in aircraft windshield structure against Bird Strike. Materials & Design*, 31(2), 687–695.

[23] Hedayati, R., & Sadighi, M. (2016). *Finite element bird-strike modeling*. Bird Strike, 113–159.

[24] Qu, H., Liu, W. D. (2011). Theoretical calculation of β transition temperature of ti-6al-4v from valence electron level. Advanced Materials Research, 299-300, 592–595.

[25] Bakalis, D. P., Stamatis, A. G. (2011). Data Analysis and performance model calibration of a small turbojet engine. Proceedings of the Institution of Mechanical Engineers, Part G: Journal of Aerospace Engineering, 226(12), 1523–1533.

[26] Lakshman, N., Raj, R., & Mukkamala, Y. (2014). *Bird strike analysis of jet engine Fan Blade*. 2014 IEEE Aerospace Conference.

[27] Kermanidis, T., Labeas, G., Sunaric, M., Johnson, A. F., & Holzapfel, M. (2006). *Bird strike simulation on a novel Composite Leading Edge Design.* International Journal of Crashworthiness, 11(3), 189–202.

[28] Walvekar, V., Thorbole, C. K., Bhonge, P., Lankarani, H. M. (2010). *Birdstrike analysis on leading edge of an aircraft wing using a smooth particle hydrodynamics bird model*. Volume 1: Advances in Aerospace Technology.

[29] Carney, K. S., Pereira, J. M., Revilock, D. M., & Matheny, P. (2009). *Jet engine fan blade containment using an alternate geometry.* International Journal of Impact Engineering, 36(5), 720–728.

[30] Ran, J., Jiang, F., Sun, X., Chen, Z., Tian, C., Zhao, H. (2020). Microstructure and mechanical properties of ti-6al-4v fabricated by electron beam melting. Crystals, 10(11), 972.

CURRICULUM VITAE

Name Surname : Mert YAĞIZ

EDUCATION :

- **B.Sc. :** 2018, Istanbul Technical University, Mechanical Engineering Department, Manufacturing Engineering.